Tutor/s

Dr. Miguel González Pérez
Departament de Ciència de Materials i
Química Física

Grau
de
Química

Treball Final de Grau

Chemistry involving superfluid helium nanodroplets as a solvent.
Química implicant nanogotes d'heli superfluid com a dissolvent.

Eloi Sanchez Ambros
July 2020

UNIVERSITAT DE
BARCELONA

B:KC Barcelona
Knowledge
Campus
Campus d'Excel·lència Internacional

Les següents línies les vull dedicar a aquelles persones que han fet possible, d'una manera o altra, que hagi pogut fer aquest treball i, per tant, es mereixen els meus agraïments i molt més.

A en Miguel, per haver dedicat el seu temps personal per formar-me acadèmicament i orientar-me sempre que ho he necessitat. A tots els meus amics de la facultat, amb qui he compartit incomptables hores en classes, laboratoris, biblioteca, menjadors i bar. A en Pau, que ha sigut el meu millor amic des de que tinc memòria i sempre m'ajuda a desconnectar quan ho necessito. A la meva parella Laura, que de manera incansable m'empeny a perseguir allò que més vull i confia més en mi que jo mateix. I als meus pares i a la meva germana, Xavier, Míriam i Alba, per haver tingut la paciència d'educar-me fins ser la persona que soc.

A tots vosaltres, moltes gràcies.

REPORT

CONTENTS

1. SUMMARY

In the early 1960s, a way to synthesize superfluid helium nanodroplets was found, and in 1990 the capture of atoms and molecules by helium nanodroplets was reported for the first time. In this work, an introduction into the field of the doped superfluid helium nanodroplets is given with emphasis on the chemical perspective. The fundamental background of all the aspects discussed is explained, always keeping in mind that the aim of this work is to provide a first contact to this interesting but intricate topic. Here, we present a brief introduction on the superfluid helium nanodroplets, followed by a review on the most important experimental and theoretical methods available to investigate these systems.

In the experimental section, the most relevant techniques used to extract information from helium nanodroplets are shown. Spectroscopic techniques allow to elucidate the structures of the impurities in the nanodroplets. Pump-probe laser techniques provide a way to determine dynamic information that deepens our insight on very low-temperature chemical reactions among other processes. The special properties of helium nanodroplets allow us to find new products, such as metastable pre-reaction complexes, cold-channel products and even complex nanostructures unobtainable otherwise.

In the theoretical section, the different methods available to simulate chemical phenomena occurring within helium nanodroplets are reviewed. Fully quantum mechanical structure calculations are beyond the computational possibilities for nanodroplets of hundreds or thousands of He atoms and the description of the systems must be carried out employing a hybrid approach. In structure investigations helium nanodroplets are described using density functional theory, while the impurities (atoms or molecules) can be described employing *ab initio* or classical approaches depending on the system studied. Dynamic studies have recently been developed using similar hybrid methods. Generally, the impurities are described using quantum or classical mechanics and the superfluid helium is described using time dependent density functional theory. Several methods that use different approaches can be applied to investigate processes involving doped helium nanodroplets.

2. RESUM

Als inicis de la dècada del 1960, es va trobar una forma de sintetitzar nanogotes d'heli superfluid, i al 1990 es va reportar per primera vegada la captura d'àtoms i molècules per les aquestes nanogotes. En aquest treball es fa una introducció al camp de les nanogotes d'heli superfluid dopades, amb especial èmfasi en la perspectiva química. També es donen els fonaments necessaris per entendre els temes tractats, tenint en compte en tot moment que l'objectiu d'aquest treball es proporcionar un primer contacte amb aquest interessant però complicat camp. En les següents pàgines, presentarem una breu introducció a les nanogotes d'heli superfluid, seguida d'una revisió dels mètodes experimentals i teòrics disponibles per investigar aquests sistemes.

En la part experimental, es donen les tècniques més rellevants utilitzades per extreure informació de les nanogotes d'heli. Les tècniques espectroscòpiques permeten desxifrar les estructures de les impureses dins les nanogotes. Mitjançant mètodes làser de "pump-probe" podem extreure informació de la dinàmica de les reaccions químiques a baixes temperatures, a més d'estudiar altres processos. Les propietats especials de les nanogotes d'heli ens permeten trobar nous productes, com complexos de pre-reacció metaestables, productes resultats de reaccions a baixes temperatures i, fins i tot, complicades nanoestructures que no poden obtenir-se de cap altra manera.

A la secció teòrica, es mostren els diferents mètodes disponibles per simular processos químics que tenen lloc a les nanogotes d'heli. Els càlculs d'estructures de nanogotes de centenars o milers d'àtoms d'heli i no es poden obtenir mitjançant només mecànica quàntica, ja que són massa cars computacionalment. Cal recórrer a mètodes híbrids, on les nanogotes es descriuen mitjançant la teoria del funcional de la densitat i les impureses (àtoms o molècules) es poden considerar mitjançant mètodes de mecànica clàssica o *ab initio*, en funció del sistema estudiat. El estudis de dinàmica s'han desenvolupat recentment, utilitzant mètodes híbrids similars. En general, les impureses es descriuen utilitzant mecànica quàntica o clàssica, mentre que l'heli es descriu utilitzant la teoria del funcional de la densitat depenent del temps. Diversos mètodes de dinàmica es poden aplicar per investigar processos en les nanogotes d'heli dopades.

Paraules clau: Nanogotes d'heli superfluid, dissolvent quàntic, baixa temperatura, processos químics.

3. INTRODUCTION

3.1. HELIUM AND SUPERFLUIDITY

During a solar eclipse in 1868, the spectrum of the Sun was recorded for the first time, providing the first evidence of the helium element. It was not until 1882 that L. Palmieri found the same evidence from measurements of the lava of the Mount Vesuvius, being this the first time that helium was detected on Earth [1].

H. K. Onnes was the first one to liquify helium in 1908 [2]. It was found that two different liquid helium phases existed, one above 2.17 K (at 1 atm), named Helium-I, and one below, named Helium-II [3,4]. This phase transition presented some interesting properties, for instance, a maximum in the liquid density and a very high peak in its heat capacity [5].

However, the most important property of Helium-II is its superfluid behaviour. Below the transition temperature, named critical temperature or T_λ, a fraction of the atoms exists in their lowest possible energy level that can be described by a collective macroscopic wavefunction, i.e. they behave as a Bose condensate.

The information given refers to ^{4}He specifically, but there is another isotope of helium found in nature, ^{3}He. The behaviour of the two isotopes differs vastly due to their different nature. ^{3}He is a fermion and cannot normally form a Bose condensate. Interestingly, superfluid behaviour is observed at temperatures below 0.003 K, when ^{3}He atoms can form pairs that become bosons, being able to behave as a condensate [6]. Furthermore, let us note that ^{3}He is ~10^6 times less abundant than ^{4}He [7], which limits its practical applications.

In 1938 Tisza proposed the two-fluid model, which considers helium as a mixture of a normal liquid and a condensate following different behaviours [8]. Three years later Landau extended this idea considering the elementary excitations of a quantized liquid, phonons and rotons. The superfluid could be described as a fraction being in its fundamental state and another fraction that was excited. Landau proposed that below a critical velocity, namely, Landau's critical velocity, no elementary excitations occurred, and a friction-less flow took place. In the case of ^{4}He this velocity is around 58 m·s^{-1} [9]. Note that Landau did not relate superfluidity with Bose condensates at any

point. It was Bogoliubov, in 1947, who proved that in a Bose-Einstein condensation there are no individual particle excitations but only collective modes, a situation in which superfluidity could arise [10].

3.2. HELIUM NANODROPLETS

Due to the extremely low interaction of helium with other substances, helium is a rather bad solvent. In fact, the substances will interact significantly more with the surfaces of the container and the impurities of the liquid than with the helium itself. Thus, alternatives must be found to use helium as a cryogenic agent for atoms or molecules, where these species cannot interact with anything else than the helium. This is accomplished removing completely the helium container and using helium droplets instead.

The scheme of a typical apparatus used to generate helium droplets is depicted in Figure 1. By creating a pressure difference between the helium compartment and the chamber where the nozzle is, a flow of helium will appear. This was first made by Becker in 1961, who already studied the dependence of some properties of the droplets with the temperature [11].

The nozzle must be at very low temperatures in order to obtain helium droplets (roughly between 10 and 40 K depending on the pressure difference applied). When the atoms flow through the cold nozzle they condensate in aggregates of several thousands of atoms. Aggregates travelling through the low pressure chamber undergo evaporative cooling, until an equilibrium temperature is reached (0.37 K for ^{4}He and 0.15 K for ^{3}He) [6,9]. The droplets cool down to around 1 K within less than 10^{-8} s, arriving at the steady temperature in about 10^{-3} s [12]. The higher the temperature of the nozzle is the more atoms will evaporate from the droplet and, consequently, the smaller the droplets will be.
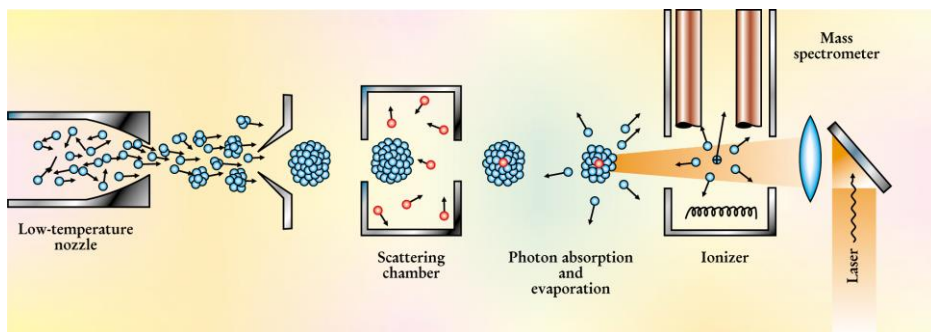

Figure 1. Schematic representation of a spectroscopic experiment with helium nanodroplets [13].

Furthermore, since this process is statistical, a distribution of different sizes of droplets will be obtained, which can be described by a log-normal distribution ($\Delta N \approx \frac{\langle N \rangle}{2}$, i.e. the width of the distribution is proportional to the size of the droplets). The diameter of the droplets ranges from 1 to 10 nm, and are usually referred to as nanodroplets.

Note that, in the case of ^{4}He the temperature of the nanodroplets is significantly below the critical temperature. Hence, the droplets are constituted by superfluid helium, and possess some interesting properties that will be discussed in the following sections.

4. OBJECTIVES

This work aims to provide an introduction to the field of superfluid helium nanodroplets, delivering a collection of the most relevant literature from its beginning to the present day. Moreover, our main focus will be the chemical perspective of helium nanodroplets and all the available experimental and theoretical methodologies available to study them.

Initially, we will review the most important and generally used experimental techniques. Then, the theoretical approaches will be presented. Along these two sections, the chemical processes of interest will be described, using practical examples in the explanations of the techniques and methods reviewed.

5. EXPERIMENTAL TECHNIQUES

Chemistry is an empirical science; hence, its foundations rely on the information extracted from natural processes. The helium nanodroplet field is not different, and over the years, different experimental techniques have been designed and optimized in order to probe these systems.

In this section, the most common and generally used techniques to study the chemical phenomena involving helium nanodroplets will be presented and discussed. A general scheme of these techniques is presented in Figure 2.
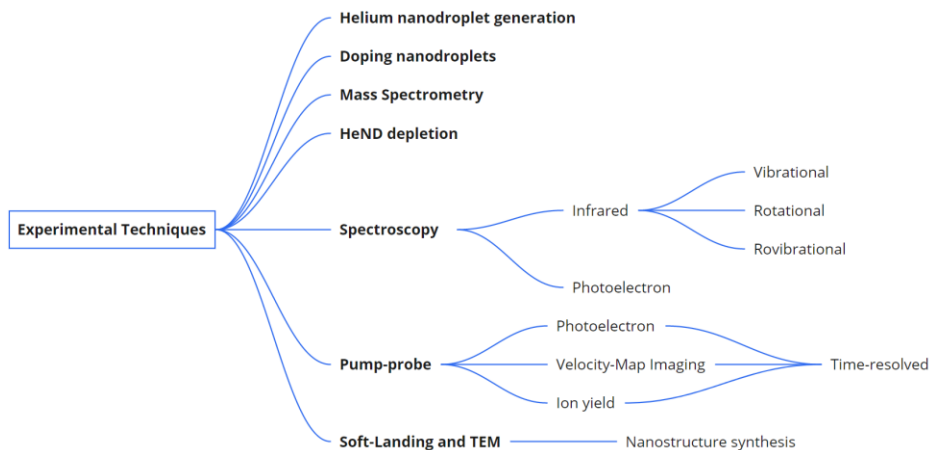
Figure 2. Scheme of the experimental techniques discussed in this work.

5.1. DOPING NANODROPLETS

Liquid helium and helium nanodroplets are remarkable systems, having properties and behaviours worth studying by themselves. However, as chemists we may ask ourselves how we can take advantage of these properties to find new chemical applications or synthetic routes.

By introducing other molecules, namely, impurities or dopants, inside the nanodroplets, we can study how a very cold and inert matrix affects them. It was 1990 when Scheidemann and Toennies reported the first doping experiment, where they found that helium nanodroplets (HeNDs) captured single atoms [14]. The same year, the capture of several other species and a comparison between three capture methods was published by the same group, which indicated that the setup shown in Figure 1 was the optimal [15].

The position of the impurity in the nanodroplet depends on the strength of the interaction between the helium and the dopant and the energy required to create a cavity in the droplet. Thus, if the capture takes place, the impurity can be fully solvated inside the droplet or reside in its surface, leading to a dimple structure. F. Ancilotto *et al*. [16] provided an equation to predict the position of the impurity based on the well depth and position of its interaction potential with helium.

Once the doping process was readily achievable, the effects of the superfluid helium environment on the molecules placed inside could be studied. A number of experimental techniques have been developed to examine these systems.

5.2. MASS SPECTROMETRY

Mass-spectrometry (MS) is one of the most used techniques in chemistry. Briefly, a sample is ionized, usually *via* electron bombardment. Then, aided by a magnetic field or an electric potential field, in case we use circular paths to divert the ions [17] or we use a Time-of-Flight-MS (TOF-MS) [18], respectively, the ions are accelerated until they arrive at the detector. The acceleration suffered by the ions is proportional to the charge to mass ratio (z/m). Since the acceleration of each ion of different charge to mass ratio is different, they can be separated and identified.

This technique is used in many fields of science in order to identify the components of a sample. However, there are some particularities that must be noted when working with helium nanodroplets. When doped nanodroplets are bombarded with electrons a wide variety of processes involving ionization can occur.

Contrarily to a gas sample of molecules being ionized, we have droplets of thousands of helium atoms doped with one or more impurities. When the droplet is ionized the charge can be localized in the impurity or in the helium. Besides, charge transfer among different species is also possible and small ionic clusters can appear. These ions will generate a signal in the detector and it is possible that groups of helium atoms form clusters by themselves (He_n), releasing the impurities along the way. If it is the impurity that holds the charge, it may form clusters with variable number of helium atoms or other reactants, yielding different signals. Furthermore, as the doping process is statistical and not all the droplets will have captured the same number of reactants from the doping chambers, the detection of nanodroplets containing by-products is unavoidable.

The resulting mass spectra are complex and hard to interpret. A common way to facilitate their interpretation is to subtract the spectra of the droplets doped with a single reactant, as was done, for instance, by S. A. Krasnokutski and F. Huisken (Figure 3) [19]. The peaks due to the He_n cluster formation and those of Si have a negative signal, indicating that they were more abundant in the Si doped droplets than in the droplets doped with both reactants. Thus, we can identify if the reaction takes place and what are the products that are obtained.
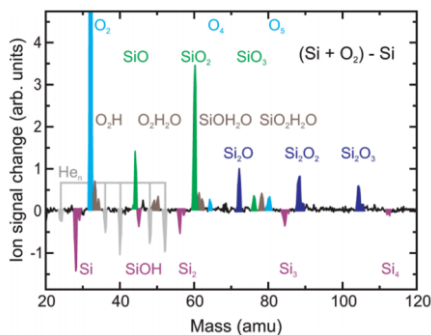

Figure 3. Differential mass spectra obtained from subtracting the Si doped HeND spectrum to the Si and O_2 doped HeND spectrum. Adapted from [19].

5.3. HELIUM NANODROPLET DEPLETION

It has already been mentioned that helium nanodroplets, though very inert, are capable of taking and then releasing the energy of the impurities upon capture. In fact, given the proper energy exchange mechanism, helium nanodroplets can facilitate the relaxation of excited impurities (see section 6.2.4). The excess energy transferred to the helium will be rapidly released *via* evaporation of some helium atoms, reducing the size of the nanodroplet accordingly. Given that the energy of evaporation per atom is known (7.2 K per ^4He atom [20], where 1 K = 0.695 cm^{-1} [21]), the energy released in a process can be estimated.

This technique, namely, helium nanodroplet depletion, allows probing whether a reaction takes place. Note that this is only possible if we find a way to relate a measurable signal with the number of atoms of the nanodroplets. The signal can be measured using the pressure due to the nanodroplets in the detection chamber, as was done by Krasnokutski and Huisken (Figure 4).
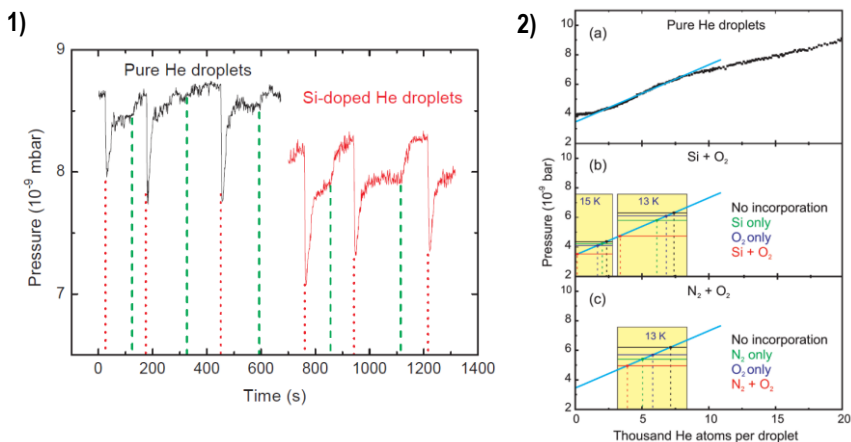
Figure 4. 1) Raw depletion measurements of pure (black) and Si-doped (red) HeND being doped with oxygen. Red dotted-lines and green dashed-lines indicate when the oxygen valve opened and closed respectively. The depletion peaks on the opening of the valve are attributed to the excess oxygen on the dead volume accumulated when the valve was closed and are not considered. 2) a) Fitting used to perform depletion measurements. b) Measurements showing a reaction between Si and O_2. c) Measurements showing no reaction between N_2 and O_2. [19]

If we compare the decrease on the number of atoms of the droplets due to the capture of each of the reactants alone and the decrease when both reactants are captured simultaneously, it is possible to, not only know if a reaction took place, but also to estimate the energy released in the reaction, though this estimation must be approached carefully due to the statistical nature of the capture process and the complexity of the process itself.

Usually, it is best to compare with tabulated thermodynamic data to choose among different possible reactions. By comparing their depletion results with previously reported data, Krasnokutski and Huisken [22] identified that the reaction of Al with O_2 inside HeNDs yielded AlO_2 instead of AlO. Similarly, the same authors [23] used this technique to identify that the reaction of carbon atoms with H_2 inside HeNDs generated a lineal HCH instead of an angular CH_2. This result differs of what is found in gas phase and room temperature, hence, the HCH generation corresponds to a cold exit channel of the reaction (see next section).

Furthermore, depletion techniques are used to prove that the reactions take place when the reactants are captured by the nanodroplets, previous to the ionization in the mass spectrometry measurements, since there are cases where the reactions are induced upon ionization (see section 5.5)

5.4. SPECTROSCOPIC TECHNIQUES

Spectroscopy is widely used to extract information from molecules. In the present case it is generally used with two different objectives: to investigate the interaction of the impurities with their environment as well as the geometry they present.

5.4.1. Infrared Spectroscopy

As previously mentioned, the superfluidity of the liquid helium leads to interesting properties in its nanodroplets. The first evidence of these properties was given in 1995 [24], when the IR spectrum of an octahedral SF_6 molecule embedded in a ^4He nanodroplet was recorded (Figure 5a). The characteristic sharp lines of a freely rotating SF_6 molecule were found. This fact could be due either to the superfluidity of the matrix or to the very low van der Waals interactions.

It was in 1998 when J. S. Grebenev *et al*. [25] recorded the IR spectrum of the OCS molecule embedded in ^3He/^4He nanodroplets with different ratios of the two isotopes. If the sharp rotational lines were due to the weak van der Waals interaction they would be observed with ^3He as well (Figure 5b).
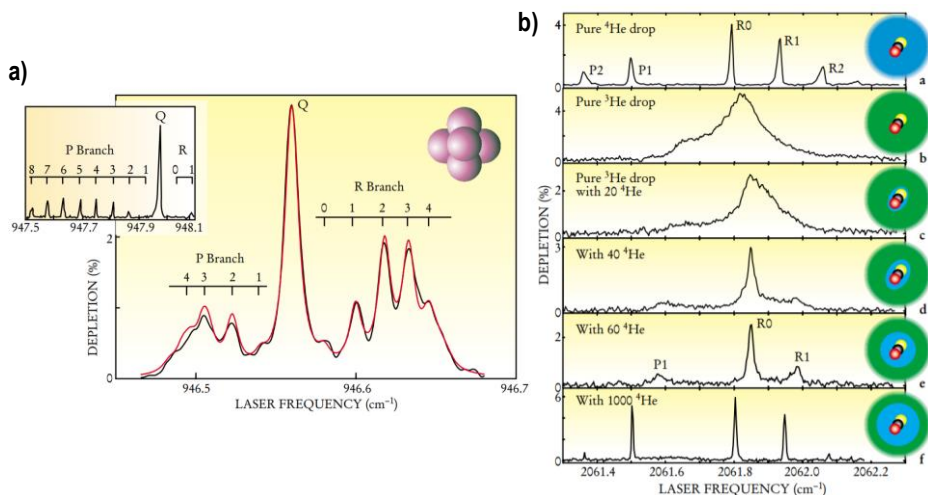
Figure 5. a) IR spectrum of the SF_6 molecule in a HeND. b) IR spectrum of the OCS molecule in HeNDs of varying ratios of ^3He/^4He. Figures from [13,24,25].

For a pure ^3He droplet, a single broadband was seen, analogous to what would be found in a classical solvent. When ^4He was gradually introduced into the droplet, the spectrum started to show the resolution of the rotational bands until it was almost identical to the freely rotating

molecule. Hence, the sharp lines of the rotational spectrum were due to the superfluidity of the [4]He droplets and not only as a consequence of the extremely weak van der Waals interactions between the impurity and its matrix.

This does not mean that the interaction of the impurity and the [4]He is non-existing. However, the little effect that [4]He has on the impurity makes it a remarkable spectroscopic matrix. The narrow spectral lines and their low shifts with respect to the free molecule make it easy to compare them with the results of *ab initio* calculations, allowing comparisons of different theoretical geometries and their spectrum with the experimental results.

For instance, two isomers were identified as the products of the reaction between the ethyl radical and an oxygen molecule inside helium nanodroplets. The authors used IR spectra predictions to assign the experimental data obtained [26].

Another example is found in the study of the aluminium reaction with HCN, where the origin of a small red shift on the spectrum was successfully attributed to the formation of a bent Al-HCN product. In this geometry the p-electron of the aluminium was delocalized into the antibonding molecular orbitals of the HCN fragment [27].

The low temperature of helium nanodroplets is also useful to study reactions in very cold environments, allowing to simulate the conditions of the interstellar medium. When impurities are captured, they are rapidly cooled down to the HeND equilibrium temperature (0.37 K), and in this conditions, uncommon products can be found due to the low energy of the reactants. There are cases where the reactants cannot overcome the first reaction barrier and are trapped in a pre-reaction complex that can provide us insight on the initial part of the reaction. In other cases, the normal gas phase reaction takes place until it is stopped at some point, providing new cold exit channels for the reactions (see reference to [23] in the previous section).

An example of this is given by J. T. Brice *et al.* [28] in their study of the reaction between HCN and the oxygen atom. A linear O-HCN pre-reaction complex was identified using IR spectroscopy and comparison of the results with theoretical calculations. In this case the reaction does not take place, since the reactants do not have enough energy to overcome the first barrier.

Another example of this phenomenon was found by K. Nauta and R. E. Miller [29] when studying highly polar molecules in HeND. Self-assembly of HCN linear chains of up to seven molecules was found using IR spectroscopy, though HCN molecules tend to form more stable cyclic trimeric structures. The linear clusters were trapped in a local minimum due to the very low

temperature of the environment, even though a lower energy minimum was available. Here, the linear product is a cold channel of the reaction.

Many cases can be found where IR spectroscopy has been used to study the outcomes of reactions taking place inside helium nanodroplets. Some other examples apart from the ones already given are [30–32].

5.4.2. Photoelectron Spectroscopy and REMPI

Another highly utilized technique is photoelectron spectroscopy, where the impurities are ionized, and information of the system can be extracted by analysing the energy of the ejected photoelectrons. Due to the high frequency required to ionize most species using a single photon, it is usually best to perform multiphoton ionizations using less energetic light, since many ambient species can absorb at high-UV [33].

Resonance-enhanced multiphoton ionization (REMPI) uses multiple photons to achieve ionization (Figure 6a). The energy of a photon (or the sum of some of them) is equal to the energy required to bring the impurity to a highly excited energy state. From that state, another excitation will readily ionize the impurity, ejecting a photoelectron that will be detected. The standardized nomenclature of (n+1) REMPI, means that n photons are used to excite the molecule and 1 electron is used to ionize it.
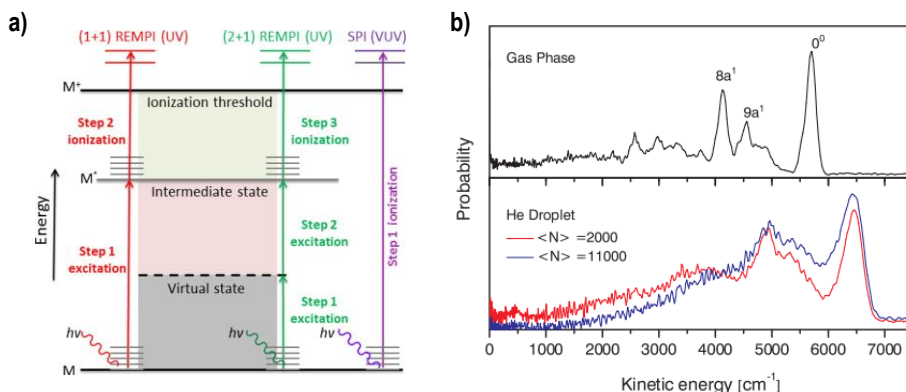

Figure 6. a) Scheme of REMPI and single photon ionization processes [33]. b) Photoelectron spectra of aniline in gas phase (top) and inside HeNDs of different sizes (bottom) [34].

Several factors can modify the energy of the photoelectron when comparing it with the gas phase REMPI. The energies of the electronic states of the states can be altered due to interactions

with the helium, though, equally to the IR spectroscopy case, the shifts are small and usually identifiable. Besides, if the impurity is fully embedded in the nanodroplet the ejected photoelectron will require to pass through some helium density to arrive at the detector. This process produces small and predictable modifications to the photoelectron energy that depend on the nanodroplet size.

This was reported by E. Loginov *et al.* [34] by studying the photoelectron spectra of aniline doped HeND and comparing it with the gas phase analogous. As can be seen in Figure 6b, the peaks are blue-shifted due to the dipole interaction of the aniline with the liquid helium. Furthermore, the peaks are asymmetrically broadened to lower energies due to the loss of energy of the photoelectrons when traversing the helium nanodroplet. Finally, for droplet radii of 38 Å or more there is an almost absolute disappearance of low energy electrons. The authors speculate that at these low energies the electrons could be trapped in the helium density and eventually recombine with the aniline cation.

The photons are usually generated using a single source. Consequently, they all possess the same energy. However, there are cases where two different sources can be used (two-colour REMPI). An example of use of this method can be seen in the work of F. Lindebner *et al.* [35], that used two-colour REMPI to detect Cu atoms captured by the nanodroplets.

If a high ion or photoelectron yield is required, the REMPI technique yields better results than single photon ionization. Its use is so widely generalized that it has become a tool in other situations that require the ionization of the studied species, such as velocity-map imaging (see next section) or mass spectrometry (see section 5.2)

5.5. PHOTOINDUCED PROCESSES AND PUMP-PROBE TECHNIQUES

Photoinduced processes are of major importance in many fields of science and are used in a large number of applications. Furthermore, they play an essential role in lots of bioprocesses such as the photosynthesis in plants or the obtention of vitamin D in humans. The field of helium nanodroplets is not an exception to this, and photoinduced processes present interesting properties.

5.5.1. Time-Resolved Photoelectron Detection

The dynamics of photoinduced processes can be studied using pump-probe techniques. The initial excitation, namely, the pump, brings the system to an excited state, and a process begins

to occur. We can probe the system using another irradiation delayed by an interval of time. By repeating the experiment (always replicating the same conditions) and changing the delay between the pump and the probe lasers, the evolution of the system over time can be resolved. Note that the probe must be designed to extract information of an observable that changes over time once the first excitation has occurred.

To demonstrate the potential of this technique we can refer to the works of B. Thaler *et al*. [36] and [37]. When indium atoms are excited from the 5s^2 5p ($^2P_{1/2}$) state to the 5s^2 6s ($^2S_{1/2}$) they evolve from a heliophillic state, where the atoms are fully immersed in the nanodroplet, to a heliophobic state that results in their ejection. Furthermore, the excitation increases the volume of the valence orbital of the In atom, causing the bubble placed around the atom to expand due to the increased interaction with the surrounding helium (Figure 7a).

Figure 7b shows the photoelectron energy for laser probe delay times up to 1 ps when the initial radiation was of 360 nm, corresponding to the purple arrow in Figure 7a. The ejected photoelectron loses energy when increasing the delay time, indicating the speed at which the helium bubble surrounding the impurity is expanded. At around 600 fs the energy stabilizes, suggesting that the bubble has stopped expanding.

When studying at a longer time-scale (Figure 7c), i.e. up to 200 ps of delay between the laser pump and probe irradiations, an oscillation on the photoelectron energy can be observed. The results were fit to the sum of an exponential function and a Gaussian function of time centred around the oscillation maximum (t_{osc}). The oscillation peak corresponds to the bubble contracting after the initial fast expansion. In all cases it lies around ~30 ps, although there is slight increase of this time when the energy of the initial excitation increases.

The In$^+$ ion yield recorded in a TOF-MS is depicted, in Figure 7d. It remains constant for almost 40 ps, increasing constantly after that. The increase is attributed to the ejection of the In atoms from the droplets. The results are fitted to a Heaviside function (accounting for the initial *plateau* with the parameter t_{ejec}) multiplying an exponential increasing function, and do not show a clear tendency, suggesting that the ejection process is independent of the initial excitation energy.

A related work was recently published [38] where an heliophilic In$_2$ dimer solvated within the droplet was excited to a coherent superposition of vibrational heliophilic states. In addition to the ejection of the dimer, the dynamics of its vibrational wavepacket were also studied.
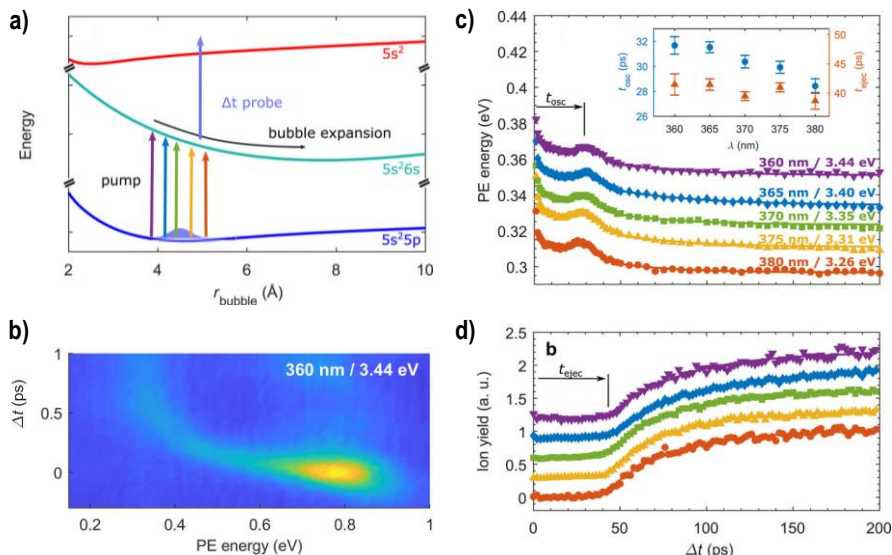
Figure 7. a) Scheme showing the pump-probe process and the energy of the relevant states of the impurity (In) as a function of the solvation bubble size. b) Photoelectron energy over time when the initial excitation is of 360 nm. c) Photoelectron energy over time for different initial excitation energies. Each point corresponds to the maximum intensity of the photoelectron energy spectra. d) In$^+$ ion yield over time. b) c) and d) were obtained using HeND of 4700 He atoms on average. The inset in c) shows the fit t_{osc} and t_{ejec} for the different initial excitation energies. Data points for each wavelength in c) and d) are offset for better visualization. Adapted from [37].

5.5.2. Velocity-Map Imaging

As explained in previous sections, when ions are generated inside HeND, complex secondary processes and species often appear. This does not exclude the possibility of their study, as seen with all the examples where the produced ions were measured and analysed (see section 5.2). However, it is possible to study systems free of these interferences, as it will be shown with two examples at the end of this section. In such specific cases, velocity-map imaging (VMI) technique allows to determine the velocities of the species of interest.

The process starts by ionizing the compound, for instance, using REMPI. Due to the vast difference of mass between the electron and the ion generated, it is safe to assume that the velocity of the ion is unaltered by this process. A set of electrostatic fields, that act as lenses, focus the generated ions into a position-sensible detector. The detector measures the number of ions that collide at each point of its surface. The position of the ions detected depend only on their mass, their initial velocity and the electrostatic fields driving them to the detector. The 2D image

generated in the detector, can be processed using an inverse Abel transform, which yields the 3D velocity distribution of the ions at the moment of ionization (Figure 8). The intricacies of the Abel transform are far from the aim of this work, but a derivation can be found in pages 4-9 of [39] and 60-61 of [40].
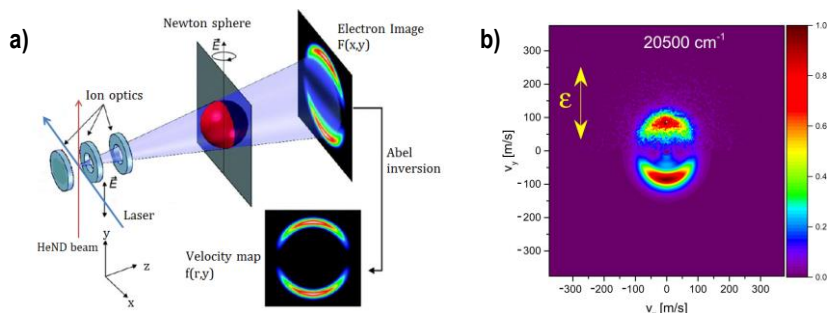

Figure 8. a) VMI instrumental setup. Adapted from [39]. b) Typical velocity distribution obtained from the photoinduced desorption of Rb_2 dimers from HeND surfaces. Top half of the image corresponds to the raw data obtained in the detector and bottom half to the result of the inverse Abel transform. The vertical arrow depicts the polarization of the laser used to ionize Rb_2 [41].

As previously stated, the use of this technique is limited to systems where the ions are, somewhat, isolated from helium. This is the case when the impurities are not fully embedded in the HeND but reside adsorbed on their surface. A. Sieg *et al*. [41] studied the Rb_2 dimer desorption from HeND when excited to heliophobic states. The dimer was irradiated with laser at different wavelengths, and the differences between the Rb_2^+ velocity distributions obtained were analysed. The authors concluded that the preferred ejection directions of the dopant were determined by the symmetry of the internal states of the molecule and not on the symmetry of the complex dopant-droplet. Furthermore, the ejection direction exhibits opposite anisotropies for Rb_2 in its singlet state than in its triplet state.

Another idea was used by A. Braun and M. Drabbels [42–44] to study the photodissociation of alkyl iodides inside HeND. First, the molecules were excited, which provoked their dissociation. Then another irradiation produced the ionization of the fragments, which were then detected. The second irradiation was delayed enough (50 ns) to ensure that, by the time of the ionization, the fragments had fully escaped from the nanodroplet. VMI was used to measure the kinetic energy of the ejected fragments from nanodroplets of different sizes, and an important dependence was found for the different molecules considered. Furthermore, VMI allowed to identify the recombination of CH_3I molecules in HeND of 31 Å of radius and bigger.

5.5.3. Time-resolved Ion Yield Detection

Another process that can be studied in HeND is quantum foam formation. When captured by HeND, impurities are surrounded by a solvation layer that, depending on the strength of its interaction with the helium, can be of significant density. This layer may act as a barrier, restricting the ability of the impurities to interact with each other. In combination with the extremely low temperature of the nanodroplets, this may completely hinder reactions from happening, and the impurities can form dispersions where they all maintain their identity (see section 6.1.1).

By excitation the atoms of the foam, it is possible for them to obtain enough energy to break the helium barriers separating them, allowing the atoms to strongly interact and aggregate. This exact phenomenon was reported by S. Göde *et al*. [45] when doping HeND with magnesium atoms. Then, when the Mg atoms were solvated, a metastable structure of individually solvated atoms was obtained. When a pulse of radiation was sent to the doped nanodroplets, the foam collapsed in Mg clusters. By performing another excitation, delayed from the previous one, and analysing the changes in the ion yield, the time of collapse was found to be ~350 fs.

5.6. SOFT-LANDING AND TRANSMISSION ELECTRON MICROSCOPY

To finish the experimental section, let us see a radically different synthetic route available thanks to the helium nanodroplets. This method is remarkably interesting in chemistry, particularly in the field of materials science, as it allows to synthesize a wide variety of nanostructures. These nanostructures are synthesized inside helium droplets and then deposited on a surface using the soft-landing approach (where the nanodroplets containing the products collide with a surface). The liquid helium spreads and evaporates, acting as a pillow that reduces the impact of the impurity with the surface. A theoretical study using time dependent density functional theory (see section 6.2.2) by N. F. Aguirre *et al*. [46] described the soft-landing mechanism that facilitates the non-destructive deposition of the clusters.

Once the product is deposited on a surface it can be characterized. The most common technique is transmission electron microscopy (TEM), which allows to directly observe the size and shape of the particles obtained. The characteristics of the nanostructures obtained may be modified by the reaction conditions, e.g. pressure in the doping chamber, temperature of the nozzle that generates the nanodroplets, order of capture of the reagents, etc.

P. Thaler *et al*. [47] thoroughly studied the effects of the reaction conditions on the formation of Au and Ag clusters inside helium nanodroplets. One of the most interesting observations was

found when changing the temperature of the nozzle from which helium is expanded. At a helium pressure of 20 bars in its chamber, when the temperature of the nozzle was 7 K the Au clusters present spherical shapes. Instead, when the temperature was set to 8 K, the appearance of elongated Au clusters is observed, which indicated the existence of a transition temperature between the two forms.

One of the most important potential applications of helium nanodroplets is to provide a new synthetic route to metal nanowires. This possibility was first reported by L. F. Gomez *et al*. in 2012 when doping HeND with Ag atoms [48]. After the soft-landing deposition of 1000 nm diameter droplets, trails of Ag nanorods were observed (Figure 9.1). This was attributed to the formation of quantum vortices in the HeND in the moment of their formation that facilitated the ordering of the impurities along their axis, generating nanowires that fragmented when deposited.

D. Spence *et al*. [49] reported the successful deposition of nanowires without any fragmentation in 2014. This was found by sequentially doping HeND with Ag and Si. The formation of Si nanowires was found even in small droplets where Ag forms spherical clusters (Figure 9.2a). Furthermore, in large nanodroplets Si atoms were found to surround the Ag clusters and fill in the gaps between them (Figure 9.2b). With this information two conclusions were presented. The appearance of nanorod trails was a specific phenomenon of silver and did not translate to other elements. Also, silver did not form nanowires that fragmentated upon collision but separated clusters with elongated shape that maintained this structure when deposited.
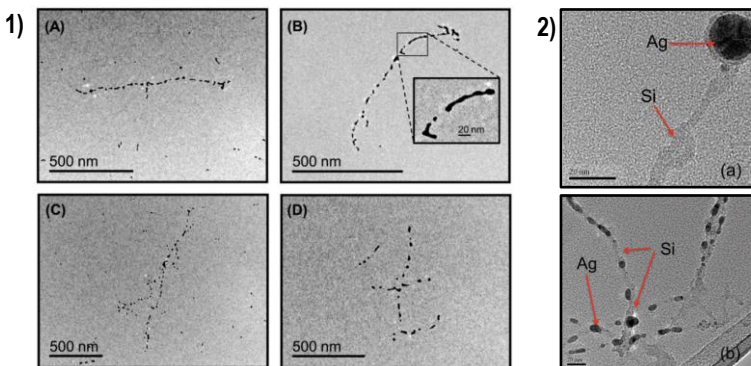
Figure 9. 1) Ag trails of nanorods synthesised in 1000 nm diameter HeND [48] 2) a) Si nanowires obtained in 250 nm diameter HeND while Ag forms spherical clusters. b) Nanowires and nanorods of Si and Ag respectively obtained in 3000 nm diameter HeND. Adapted from [49].

Later in 2014 E. Latimer *et al*. [50] reported the synthesis of Au, Cr, Ni and Si nanowires using the soft-landing method. It was further confirmed that the formation of nanorod trails was a special case of Ag, since none of the other compounds utilized displayed such behaviour.

In summary, HeND proved to be a remarkable tool with a great potential for nanostructure synthesis. By adjusting the reaction conditions the obtained products can be largely tuneable, allowing to obtain thin cluster films of elements like, for instance, Mg [51], structures of high catalytical activity [52] and metallic and non-metallic nanowires among other examples.

6. THEORETICAL METHODS

In the previous sections the remarkable properties of helium have been shown. Furthermore, different experimental techniques that have provided several ways to profit them have been described. However, science relies on theoretical knowledge as much as on empirical, and solid theoretical foundations are required to fully understand such a unique system.

In this section the main theoretical methods used to describe liquid helium environments and the molecules embedded in it will be explained, focusing on chemical systems, which are complex in nature. Thus, there will be an emphasis on the methodologies that allow this kind of studies, even though there may be others used in different contexts.

Theoretical methods can be roughly divided in two different groups, static and dynamical methods. A general scheme is presented in Figure 10.
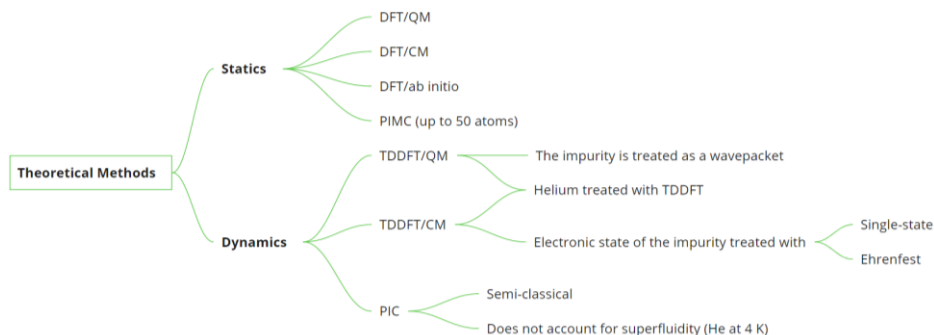
Figure 10. Scheme of the theoretical methods discussed in this work.

6.1. STATICS

Static studies provide the starting point of the theoretical studies. They are mainly used to elucidate the possible system structures and their energies. The motion equations are not propagated over the real time, though it will be shown that a propagation over the imaginary time may be useful.

6.1.1. DFT/QM and DFT/CM

The chemical systems studied can usually be thought of two distinct parts, the helium environment and the dopants placed in it. Thus, due to the different complexity of the two parts it is usually convenient to separate their treatment, utilizing the most convenient theoretical approach for each of them.

Nowadays, the most common way to treat helium is using density functional theory (DFT). This approach finds its foundations in the Hohenberg-Kohn theorems, derived in 1964 [53]. In essence, it allows to reduce the many-body problem of N electrons, which depend on $3N$ spatial coordinates, to only three spatial coordinates, drastically reducing the computational cost of the calculations.

Hohenberg and Kohn demonstrated that the properties of a non-degenerate ground state of a many-electron system are uniquely determined by the electronic density, which depends on three spatial coordinates.

In the field of liquid helium, the functionals used for the energy have the following form.

$$E[\rho_{He}] = \frac{\hbar^2}{2m_{He}} \int d\boldsymbol{R}_{He} \left(\boldsymbol{\nabla}\sqrt{\rho}\right)^2 + \int d\boldsymbol{R}_{He} \, \mathcal{E}_c[\rho] \tag{6.1}$$

Where the helium density is related to the atomic wavefunction of the N helium atoms of the system, $\rho_{He}(\boldsymbol{R}_{He}) = N|\phi_o(\boldsymbol{R}_{He})|^2 = |\psi_{He}(\boldsymbol{R}_{He})|^2$. The first term of (6.1) refers to the kinetic energy of the helium, while the other one can be split in two different contributions, the potential energy of the particles and another term accounting for the correlation.

Different forms of this expression can be used, but the most used one in the context of superfluid helium is the Orsay-Trento density functional [54]. Depending on the system studied different modifications can be made to simplify it if it is necessary to reduce the computational cost.

Provided that there is no impurity, we have to find the helium density that minimizes the energy of the system, maintaining the number of atoms constant, which in turn is also given as a functional of the density $N = \int d\boldsymbol{R}_{He}\rho_{He}(\boldsymbol{R}_{He})$. This can be achieved by solving the following non-linear Schrödinger-like equation:

$$\left[-\frac{\hbar^2}{2m_{He}}\boldsymbol{\nabla}^2 + U[\rho, \boldsymbol{R}_{He}]\right]\sqrt{\rho(\boldsymbol{R}_{He})} = \mu_{He}\sqrt{\rho(\boldsymbol{R}_{He})} \tag{6.2}$$

Where $U[\rho, \boldsymbol{R}_{He}] \equiv \delta\mathcal{E}_c/\delta\rho$ corresponds to an effective potential energy and μ_{He} is the chemical potential of helium. This equation is solvable by an iterative method and will provide the structure of a pure helium droplet of N atoms.

However, as chemists, we are interested in the processes taking place when impurities interact inside or on the surface of helium droplets. To study the system of helium droplets with

impurities we have to consider the energy of the overall system and minimize it, analogously the pure helium droplet case. The energy of a helium droplet with a dopant X is given by:

$$E[\rho_{He}, \phi] = \frac{\hbar^2}{2m_{He}} \int d\boldsymbol{R}_{He} \left(\boldsymbol{\nabla}\sqrt{\rho}\right)^2 + \int d\boldsymbol{R}_{He} \, \mathcal{E}_c[\rho] + \frac{\hbar^2}{2m_x} \int d\boldsymbol{r}_X \, |\boldsymbol{\nabla}\phi(\boldsymbol{r}_X)|^2$$
$$+ \iint d\boldsymbol{R}_{He} d\boldsymbol{r}_X |\phi(\boldsymbol{r}_X)|^2 V_{He-X}(|\boldsymbol{R}_{He} - \boldsymbol{r}_X|)\rho(\boldsymbol{R}_{He}) \tag{6.3}$$

Where equation (6.3) is equal to equation (6.1) plus the kinetic energy of the dopant (atom or molecule) and the interaction potential energy between the dopant and the helium. Upon minimization with respect to the helium density and the impurity wavefunction, two coupled non-linear Schrödinger-like equations can be found.

$$\left[-\frac{\hbar^2}{2m_{He}}\boldsymbol{\nabla}^2 + U[\rho, \boldsymbol{R}_{He}] + U_{He-X}(\boldsymbol{R}_{He})\right]\psi_{He}(\boldsymbol{R}_{He}) = \mu_{He}\psi_{He}(\boldsymbol{R}_{He}) \tag{6.4}$$

$$\left[-\frac{\hbar^2}{2m_X}\boldsymbol{\nabla}^2 + U_{X-He}(\boldsymbol{r}_X)\right]\phi(\boldsymbol{r}_X) = E\phi(\boldsymbol{r}_X) \tag{6.5}$$

Where E is the lowest eigenvalue of the energy of the impurity, U_{He-X} is the interaction potential energy of helium with the impurity and U_{X-He} is the interaction potential energy of the impurity with helium.

$$U_{He-X}(\boldsymbol{R}_{He}) = \int d\boldsymbol{r}_X \, |\phi(\boldsymbol{r}_X)|^2 V_{He-X}(|\boldsymbol{R}_{He} - \boldsymbol{r}_X|) \tag{6.6}$$

$$U_{X-He}(\boldsymbol{r}_X) = \int d\boldsymbol{R}_{He} \, \rho(\boldsymbol{R}_{He}) V_{He-X}(|\boldsymbol{R}_{He} - \boldsymbol{r}_X|) \tag{6.7}$$

Equations 6.4 and 6.5 are coupled as the U_{He} and U_X terms include the impurity wavefunction and the helium density, respectively. The solution of these equations will lead to the helium and the impurity wavefunctions simultaneously, where the wavefunction of the helium is related to its density by $\psi_{He}(\boldsymbol{R}_{He}) = \sqrt{\rho_{He}(\boldsymbol{R}_{He})}e^{i\theta}$ and θ is the global phase of the helium wavefunction.

This methodology can be generalized for an arbitrary number of impurities and is the basis of the DFT/QM structure calculations. Furthermore, it can be modified to treat the impurities classically, as we will see in section 6.2.2.

6.1.1.1. Imaginary Time Propagation

Equations (6.4) and (6.5) are usually solved using the Imaginary Time Propagation (ITP) method [55]. The solutions to the time-dependent Schrödinger equation (TDSE), $\Psi(r, t)$, can be written as:

$$i\hbar \frac{\partial \psi(r,t)}{\partial t} = \widehat{H}\psi(r,t) \rightarrow \psi(r,t) = \sum_{k}^{\infty} c_k \phi_k e^{\frac{-iE_k t}{\hbar}} \tag{6.8}$$

$$\widehat{H}\phi_k = E_k \phi_k \tag{6.9}$$

Where the solution, $\Psi(r,t)$, of the TDSE is expressed as a linear combination of the eigenfunctions obtained from solving the time-independent Schrödinger equation (TISE). If we now consider the change $t \equiv -i\tau$, namely, a Wick rotation, we can rewrite the equations in (6.8) obtaining:

$$\hbar \frac{\partial \psi(r,\tau)}{\partial \tau} = -\widehat{H}\psi(r,\tau) \rightarrow \psi(r,\tau) = \sum_{k}^{\infty} c_k \phi_k e^{\frac{-E_k \tau}{\hbar}} \tag{6.10}$$

Note that the TDSE in imaginary time, (6.10), converges to the ground state function in the limit where $\tau \rightarrow \infty$, as all the other terms from the wave function decay exponentially faster due to their higher energy levels. The ITP method yields the ground state wave function only if the initial guess has a non-zero projection on the ground state, i.e. $\langle \psi_0 | \psi(r,0) \rangle \neq 0$. In general, equation (6.8) is integrated numerically until convergence, but other methodologies involving the time propagation operator method can be used too [56,57].

The ITP method is widely used by the groups that perform structure investigations. For instance, J. Eloranta has used DFT/QM and DFT/CM to study liquid helium with different dopants. An example of this is his study of the solvation of neon atoms in bulk superfluid helium [58].

The neon wave functions are approximated to spherical densities positioned at the centre of each atom, and the helium density is treated with the DFT approach. To solve the equations the ITP method is used. Using this methodology but treating the impurities classically, J. Eloranta could compare the results obtained by the two approaches, quantum and classical.

From calculations performed at different Ne-Ne distances, the minimum energy path of the reaction of the neon atoms could be obtained (Figure 11a). The potential energy surface (PES) is dramatically modified from the obtained in gas phase. Furthermore, clear differences appear between the DFT/QM method and the DFT/CM method which, evidently, does not account for the zero-point energy. The appearance of local maxima and minima along the Ne-Ne coordinate allowed Eloranta to predict the existence of neon quantum foams (see section 5.5.3), where the neon atoms do not form a dimer. Instead, they exist independently surrounded by the helium solvation shell and form adducts of long bonding distance.
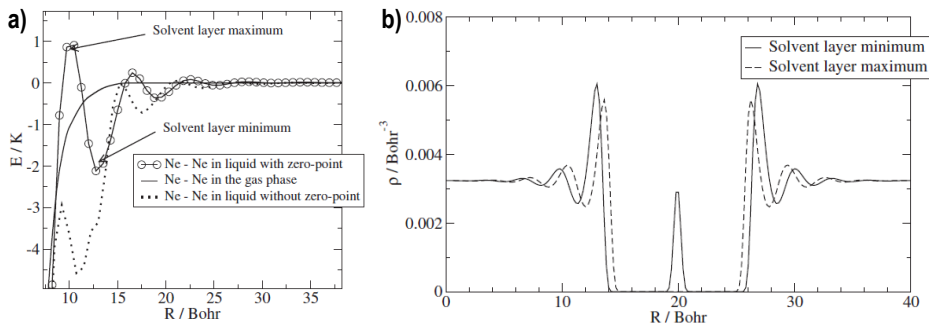
Figure 11. a) Energies along the Ne-Ne coordinate. b) Helium densities along the Ne-Ne coordinate in the minimum (Ne-Ne distance of 12.8 Bohr) and maximum (Ne-Ne distance of 10.5 Bohr) energies. [58]

Besides, the DFT/QM and DFT/CM methodologies provide the structure of the liquid helium in the presence of the dopant. The helium density along the Ne-Ne coordinate in the maximum and minimum energies is shown in Figure 11b. The presence of helium between the two neon atoms in the local minimum is clear, which insinuates the existence of a stable Ne-Ne adduct, with a 12.8 Bohr bond distance, where the two atoms are surrounded by helium density. To continue the reaction process the atoms require enough energy to remove the helium density that separates them, which may not be possible at the very low temperatures of the nanodroplets.

Even though in the previous example the wave function of the dopant was approximated to a spherical density, it can be determined by solving equations (6.4) and (6.5), as he did in his study on the solvation of fluorine atoms [59]. Applying this methodology Eloranta has studied different dopants. In some cases, he predicted that impurities could reorder establishing large bond distance crystal structures [60].

6.1.2. DFT/ab initio

Instead of working with wave packets to describe the impurity, the standard quantum chemistry approach can be used. The DFT/*ab initio* approach relies on solving the Schrödinger equation, which can only be done analytically for the one-electron systems. Consequently, a number of methods have been developed to solve more complex problems. A brief overview of the usual way of working is given next.

The Hamiltonian operator of a system of n electrons and N nuclei can be expressed as:

$$\hat{H} = \hat{T}_e + \hat{T}_N + \hat{V}_{e-N} + \hat{V}_{e-e} + \hat{V}_{N-N} = \qquad (6.11)$$

$$= -\frac{1}{2}\sum_{i=1}^{n}\nabla_i^2 - \frac{1}{2}\sum_{i=1}^{N}\frac{\nabla_A^2}{M_A} - \sum_{i=1}^{n}\sum_{A=1}^{N}\frac{Z_A}{r_{iA}} + \sum_{i=1}^{n}\sum_{j>i}^{n}\frac{1}{r_{ij}} + \sum_{i=A}^{N}\sum_{B>A}^{N}\frac{1}{r_{AB}}$$

Where $\hat{H}$ is written in atomic units, the $\hat{T}$ terms are the kinetic energy operators and the $\hat{V}$ terms are the interaction potential energy operators between the particles indicated by subscripts.

The Hamiltonian operator does not depend explicitly on time, and this allows us to separate the wave function as two parts $\psi(s_e, s_N; t) = \psi(s_e, s_N)e^{-iEt/\hbar}$, where $s_e = (r_1, \dots, r_n)$ and $s_N = (R_1, \dots, R_N)$ are the spatial coordinates of the electrons and nuclei respectively. The spatial-dependent wave function satisfies the TISE, that is, $\hat{H}\psi = E\psi$.

To solve this equation further approximations are usually required. The Born-Oppenheimer (BO) approximation takes the global wavefunction as a product of an electronic and a nucleic wavefunction, where the electronic wave function depends parametrically on the nuclei positions, $\psi(s_e, s_N) = \psi_e(s_e; s_N)\psi_N(s_N)$. In essence, it is assumed that, as the electrons move much faster than the nuclei, they can instantaneously adapt to them, allowing to write two TISE as:

$$[\hat{T}_e + \hat{V}_{e-N} + \hat{V}_{e-e}]\psi_e(s_e; s_N) = E_e(s_N)\psi_e(s_e; s_N) \tag{6.12}$$

$$[\hat{T}_N + \hat{V}_{N-N} + E_e(s_N)]\psi_N(s_N) = E\psi_N(s_N) \tag{6.13}$$

Where $E_e(s_N)$ is the electronic energy at a given nuclei geometry s_N and $\hat{V}_{N-N} + E_e(s_N) = U(s_N)$ is interpreted as the effective potential energy term of the nuclei, which includes two repulsive terms due to the nucleus-nucleus and the electron-electron interactions, an attractive term due to the electron-nucleus interactions and the kinetic energy of the electrons. The nuclear interaction potential energy is readily given by $V_{AB} = Z_A Z_B / r_{AB}$.

Equation (6.12) can't be analytically solved and many approximation methods have been developed, which can be roughly divided in two major groups: the variational and perturbational methods. Thorough explanation of these methods will not be provided here unless they are of special interest for our main topic. Nevertheless, all the cited works provide information on the methods and adaptations used, and more general content can be found in references [61,62] or other quantum chemistry books.

There are many examples of DFT/*ab initio* calculations in the literature and, usually, these studies are carried out in parallel with experimental works to gain further insight in possible structures of the products, as was explained in section 6.4 [26–28,30,63–65].

De Lara-Castells and Hauser performed a study following this methodology where they tried to find an explanation for the following phenomenon. Cesium dimers, which are heliophobic and

stay on the surface of the droplets, were found to be embedded inside the helium nanodroplets when a fullerene molecule (C_{60}) was added. It was guessed that the dimers reacted with C_{60}, which resides inside the droplet, even though their reactivity was not as high as in the gas phase. Then, the resulting ionic pair was strongly solvated and found inside the nanodroplet [66].

De Lara-Castells and Hauser [67] initially calculated the PES for C_{60} with Cs and Cs_2 in the gas phase, first allowing for full electron transfer and then fully constraining it (Figure 12a and Figure 12b, solid lines). Next, the helium density was considered by minimizing the helium structure at different dopant distances and calculating its energy (Figure 12c). The positive energy found when the dopants approach is the energy required to remove the solvation layers surrounding the dopants.

If the helium is assumed to be inert regarding the electron transfer between the dopants, the gas phase PES can be corrected by adding the energy due to the helium environment and, likewise, for the case where the interactions between the dopants are fully covalent (Figure 12a and Figure 12b, dashed lines).

It is noticeable that in the case where the electron transfer is assumed to be unmodified by the helium, the corrected PES are bonding in all cases, including the atomic Cs one. Contrarily, if the electron transfer is fully quenched the PES obtained are entirely repulsive.
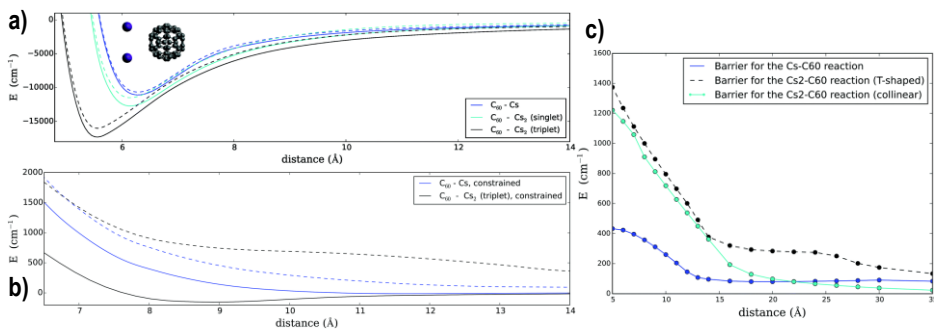
Figure 12. Interaction potential energies between C_{60} (a) and a Cs atom and Cs_2 T-conformation allowing charge transfer, (b) and a Cs atom and Cs_2 T-conformation constraining charge transfer. Solid lines are gas phase calculations and dashed lines are corrected by the helium environment as shown in (c). [67]

The authors conclude that the electron transfer process, although significantly quenched, can take place through the liquid helium separating both dopants. Further investigation was carried out in a subsequent study [68]. Helium correlation was added to the PES calculations via the

second order Møller-Plesset (MP2) perturbation method and the reaction path and reaction probabilities where calculated, finding a good agreement with the experimental data.

This example, altogether with Eloranta's studies explained before, show how static calculations are used to gain insight in the processes taking place inside helium nanodroplets. Furthermore, static studies are fundamental in dynamical studies as well (see section 6.2), where they are used to obtain the initial conditions of the system.

6.1.3. Path Integral Monte Carlo

There have been great efforts from the scientific community to obtain fully quantum mechanical results. To do so the path integral Monte Carlo (PIMC) method is used. Interested readers on this method are referred to the D. M. Ceperley review on PIMC for condensed helium [69] and to the R. Rodriguez-Cantano *et al.* review on PIMC applied to doped helium clusters [70].

The PIMC can be used to simulate superfluid bosonic systems. This method solves Feynman's path integrals, which provide a direct way of calculating thermodynamic properties of the system. The computational requirements of these calculations are significantly higher than those of the DFT approach. Thus, the clusters that can be studied can contain up to 40 helium atoms.

Due to this limitation the PIMC method is not useful to predict structures of large helium droplets but can provide a good insight on the small clusters that can be found, for instance, when helium droplets are doped with some ionic impurities. The experimental and theoretical study by R. Perez de Tudela *et al.* [71] is a good example of this. The aim of the study was to elucidate how Cs^+ ions are solvated. By means of TOF-MS the most stable He_NCs^+ clusters were identified. Interpreting the spectra and with aid of theoretical structural and energy calculations it was found that the first solvation shell contained 17 helium atoms and was particularly rigid.

6.2. DYNAMICS

The aim of dynamical calculations is to find the evolution of a system over time and simulate it as truthfully as possible. In the previous section, it has been shown how solving the TISE allowed to find the energy of a system in the ground state. By this procedure, minimum energy paths can be obtained. However, real systems may not follow these paths, instead, depending on the amount of energy that the reactants have, different outcomes may occur that cannot be predicted by non-dynamical approaches.

Take, for instance, the Ne-Ne interaction potential energy shown in Figure 11. It was calculated by minimizing the structure of the helium cluster at different Ne-Ne distances, as explained before. In other words, if we wanted to interpret it dynamically, we would have to assume that neon atoms move so slow that helium can instantly adapt to their movement, in an analogous way to the BO approximation for electrons and nuclei.

This approximation may or may not be justified depending on the conditions of the system. In capture chambers dopants travel at hundreds of meters per second and collisions with helium occur rather violently. Thus, an energy transfer from the dopant to the helium takes place, and the droplet is excited (phonons, rotons and ripplons). Evidently, this kind of processes will not be accounted for in the minimum energy path approximation and other methods must be used.

6.2.1. TDDFT/QM

Due to the complexity of the systems, fully quantum dynamical calculations are beyond the present computational possibilities. Instead, the usual procedure uses time dependent density functional theory (TDDFT) to describe helium and the QM or CM methods to describe the impurities, being CM the most commonly used.

Dynamic calculations can be formulated by generalizing the following example. Let us consider a droplet of N atoms and an atom impurity that collides with it, that is, a capture process. To find the equations governing the time motion of the system we can minimize the quantum action of the system, which is given by:

$$\mathcal{A}[\psi_{He}, \phi_X] = \int dt \left\{ E[\psi_{He}, \phi_X] - i\hbar \int d\boldsymbol{R}_{He} \psi_{He}^* \frac{\partial}{\partial t} \psi_{He} \right.$$
$$\left. - i\hbar \int d\boldsymbol{r}_X \phi_X^* \frac{\partial}{\partial t} \phi_X \right\} \tag{6.14}$$

Where $E[\psi_{He}, \phi_X]$ is the total energy of the system and is analogous to (6.3). As stated, now we must minimize the action by performing variations of the wave functions ψ_{He} and ϕ_X. This leads to two coupled non-linear Schrödinger-like equations:

$$i\hbar\frac{\partial}{\partial t}\psi_{He} = \left[-\frac{\hbar^2}{2m_{He}}\boldsymbol{\nabla}^2 + U_{He-X}(\boldsymbol{R}_{He}) + \frac{\delta\mathcal{E}_c}{\delta\rho}\right]\psi_{He} \qquad (6.15)$$

$$i\hbar\frac{\partial}{\partial t}\phi_X = \left[-\frac{\hbar^2}{2m_X}\boldsymbol{\nabla}^2 + U_{X-He}(\boldsymbol{r}_X)\right]\phi_X \qquad (6.16)$$

Where the interaction potentials U have been defined in equations (6.6) and (6.7). Note that the equations found are general for any system of a droplet with one impurity. Furthermore, the operators acting on the wave functions are, obviously, identical to the ones found in the static case for a single doped droplet. However, in the current case, we are interested in the propagation of the wave functions over the real time.

With these equations we can study any process involving a single doped helium droplet. The initial conditions will control what process will take place. In the case of a capture the initial conditions will be a pure helium droplet of N atoms and an impurity wave packet directed to the droplet with an appropriate initial velocity distribution.

This procedure, titled TDDFT/QM, was followed by A. Vilà *et al.* [72] to study the dynamics of the pick up process of neon atoms by helium nanodroplets. In this case, the movement of the impurity was restricted to the z-axis to focus in the zero angular momentum case.

In Figure 13a, snapshots of the temporal evolution of a neon atom with an initial velocity distribution of $\langle v_0 \rangle = 500 \; m \cdot s^{-1}$ are depicted, as an example of the results obtained with the described approach. From the moment of the collision the droplet shows multiple waves that travel through the liquid. The energy received by the droplet upon collision is liberated *via* evaporation of some helium atoms. At the time of 118.45 ps the first solvation layer is visibly formed around the impurity, since the droplet has liberated enough of the excess energy. Interferences in the neon wave packet are also observed in the moment of the collision but disappear once the atom is inside the droplet.
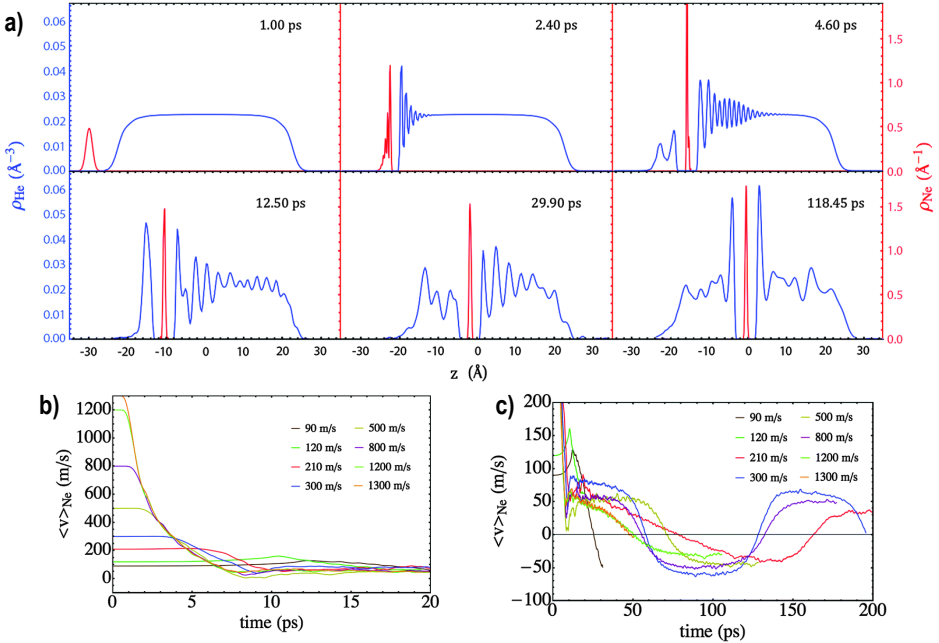
Figure 13. a) Snapshots showing the temporal evolution of the capture of a neon atom, $\langle v_0 \rangle = 500\ m \cdot s^{-1}$. b) Expected value of the velocity of neon as a function of time. c) Same as b) with different scale. [72]

The expected value of the velocity of the impurity over time for different initial conditions is shown in Figure 13b and Figure 13c. Note how, after the fast initial drop due to the impact, there are oscillations caused by the waves generated in the droplet, which are reflected on its surface and collide back with the impurity. After ~20 ps, the velocities stabilize and exhibit plateaus of almost constant velocity before stopping and changing direction. The plateaus correspond to intervals of time where the impurity travels below the Landau critical velocity and there is no friction between the impurity and the helium. When the neon atom arrives at the surface of the nanodroplet the anisotropy of the environment, and thus, the interaction potential energy, pulls it back to the centre. In A. Vilà *et al.* work [72], the calculation is propagated to the order of only a hundred picoseconds.

As stated before, the impurity was restricted to move on the z-axis only and, thus, the effect of the angular momentum is not considered. The backflow term and the non-local contribution to the helium correlation energy functional have been neglected, though this is the standard procedure when using the Orsay-Trento functional. The position and the momentum space of

both the helium density and the neon impurity was discretized using a cartesian grid, which was more or less dense depending on the initial velocity of the impurity. The higher the energy of the system, the denser the grid must be. Additionally, numerical methods must be applied in order to solve the coupled Schrödinger-like equations. The authors provide further technical information in the publication. [72]

The TDDFT/QM methodology was developed by the same group in 2015. It was initially applied to the study of the Cl_2 molecule photodissociation inside a helium nanodroplet. The quantum interferences originated in the wave packets upon collision with the walls of the cavity around the molecule, the relaxation of helium after the collision and the effect of the mass of the atoms were also investigated. [73–76]

The study of the capture process has been used as an example of application of this methodology because it was extended by M. Blancafort-Jorquera *et al.* by using the TDDFT/CM approach [77], making the comparison between the two approaches possible.

6.2.2. TDDFT/CM

The TDDFT/CM method follows the same steps as the analogous TDDFT/QM method. First, the quantum action of the system must be found, and this is given for any impurity by:

$$\mathcal{A}[\psi_{He}, \boldsymbol{r}_X] = \int dt \left\{ E[\psi_{He}, \boldsymbol{r}_X] - i\hbar \int d\boldsymbol{R}_{He} \psi_{He}^* \frac{\partial}{\partial t} \psi_{He} - m_X \left(\frac{d\boldsymbol{r}_X}{dt} \right)^2 \right\} \quad (6.17)$$

Next, the action must be minimized by taking variations to ψ_{He} and $\boldsymbol{r}_X$. This leads to two coupled non-linear Schrödinger-like equations that govern the motion of the system:

$$i\hbar \frac{\partial}{\partial t} \psi_{He} = \left[-\frac{\hbar^2}{2m_{He}} \boldsymbol{\nabla}^2 + V_{He-X}(|\boldsymbol{R}_{He} - \boldsymbol{r}_X|) + \frac{\delta \mathcal{E}_c}{\delta \rho} \right] \psi_{He} \quad (6.18)$$

$$m_X \ddot{\boldsymbol{R}}_X = -\boldsymbol{\nabla}[\int d\boldsymbol{R}_X \rho_{He} V_{He-X}(|\boldsymbol{R}_{He} - \boldsymbol{r}_X|)] \quad (6.19)$$

In Figure 14a, the velocity of the Ne atom over time is depicted [77]. Overall, the results are remarkably similar to those found in the TDDFT/QM approach (Figure 13c). After the fast decrease and initial oscillations of the velocity upon collision plateaus are found, where the atoms travel at a constant speed through the droplet. When the surface is reached, the atom is stopped and pulled back in the opposite direction.

Due to the decrease of computational requirements because of the impurity being treated classically, the effect of the angular momentum could be taken into account. This was accomplished considering an initial impact parameter (b) different from 0 (b is defined as the

distance from the centre of mass of the nanodroplet to the trajectory of the impurity before collision). The trajectories of the dopants colliding with a nanodroplet are shown, in Figure 14b. After the collision, almost elliptical trajectories were found for all impact parameters, except for those where the impurity is not captured.
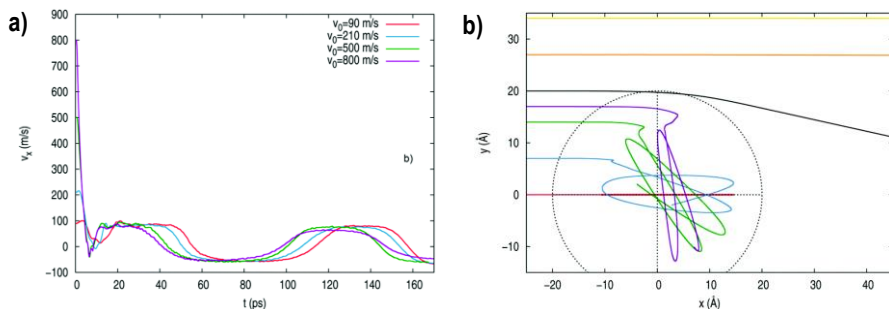

Figure 14. a) Velocity of neon atoms as a function of time. b) Trajectories of neon atoms with $v_0 = 500 \; m \cdot s^{-1}$ and impact parameter in Å of 0 (red), 7 (blue), 14 (green), 17 (magenta), 20 (black), 27 (orange) and 34 (yellow). [77]

Besides, in cases where the angular momentum of the system is high enough, the appearance of quantum vortices is induced, which proved to be a noteworthy tool for chemical synthesis (see section 5.6).

From the comparison of the results obtained by the two methods, it follows that quantum behaviour is of slight importance here (note that neon is the lightest noble gas atom that can be captured by nanodroplets). Thus, if treating this system using classical mechanics yields essentially the same results than the quantum approach, the method ought to be usable for heavier elements as well, as the quantum effects of the translational degrees of freedom will be even less significant.

When applied to more than one impurity, the TDDFT/QM and TDDFT/CM methods allow to study the dynamics of chemical reactions. A similar study to the previously described allowed to investigate the importance of quantum effects in chemical reactions inside helium nanodroplets.

A. Vilà *et al.* used the TDDFT/QM approach to study the reaction dynamics between two neon atoms (Ne + Ne@HeND) [78]. In the study, a neon atom was picked up by a single-doped helium droplet, which was in its ground state with the neon atom placed in its centre. The equations of motion were found, as in the other examples, by minimizing the quantum action of the system,

which was described by the helium wave function, ψ_{He}, a wave packet describing the relative motion of the two atoms, $\varphi_{rel}(r, t)$, and the centre of mass of the two atoms, R_{CM}:

$$i\hbar \frac{\partial}{\partial t} \psi_{He} = \left[-\frac{\hbar^2}{2m_{He}} \nabla^2 + \int dr \, |\varphi_{rel}|^2 V_{He-Ne_2}(r, \boldsymbol{R}_{He}, R_{CM}) + \frac{\delta \mathcal{E}_c}{\delta \rho} \right] \psi_{He} \qquad (6.20)$$

$$i\hbar \frac{\partial}{\partial t} \varphi_{rel} = \left[-\frac{\hbar^2}{2\mu_{Ne_2}} \nabla^2 + V_{Ne_2}(r) + \int dr \, \rho_{He} V_{He-Ne_2}(r, \boldsymbol{R}_{He}, R_{CM}) \right] \varphi_{rel} \qquad (6.21)$$

$$M\ddot{R}_{CM} = -\frac{\partial}{\partial R_{CM}} \left[\iint dr d\boldsymbol{R}_{He} \, \rho_{He} |\varphi_{rel}|^2 V_{He-Ne_2}(r, \boldsymbol{R}_{He}, R_{CM}) \right] \qquad (6.22)$$

In this treatment the impurities have been restricted to move only on one axis and their centre of mass is treated classically. Snapshots of a calculation where the colliding neon atom has an initial average velocity of $\langle v_0 \rangle = 300 \, m \cdot s^{-1}$ are presented in Figure 15. The initial snapshots are identical to what was found for the pick up process, excepting the neon atom already placed inside the nanodroplet. At 19 ps a very dense layer of helium is found separating the two Ne atoms. This density is displaced due to the high energy of the recently captured atom, which allows the reaction to take place. In the end the Ne$_2$ dimer travels through the nanodroplet as a single atom would do, and the relative distance between the two atoms behaves like a harmonic oscillator with a modified interaction potential due to the helium environment.

M. Blancafort-Jorquera *et al.* [79] extended this study using the TDDFT/CM approach, i.e. considering the impurities classically. Similar to the quantum-classical study of the Ne atom capture process, angular momenta different from zero could be introduced *via* an impact parameter of the colliding neon atom.
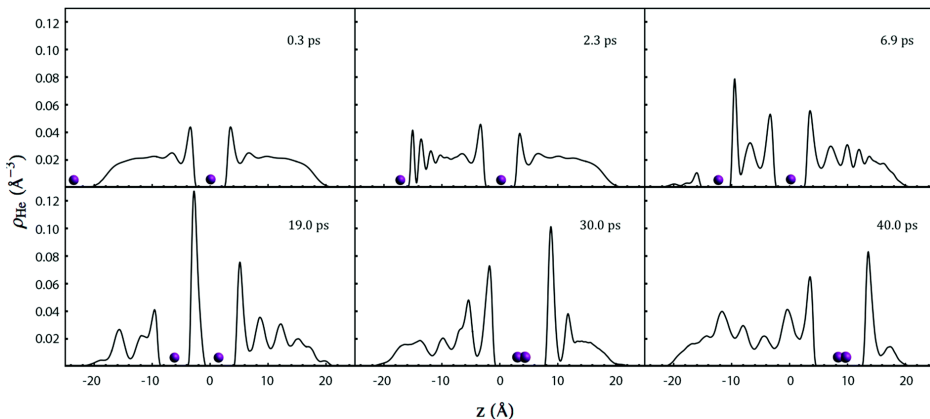

Figure 15. Snapshots of a neon atom colliding with a single-doped helium nanodroplet for an initial average velocity of $\langle v_0 \rangle = 300 \, m \cdot s^{-1}$. [78]
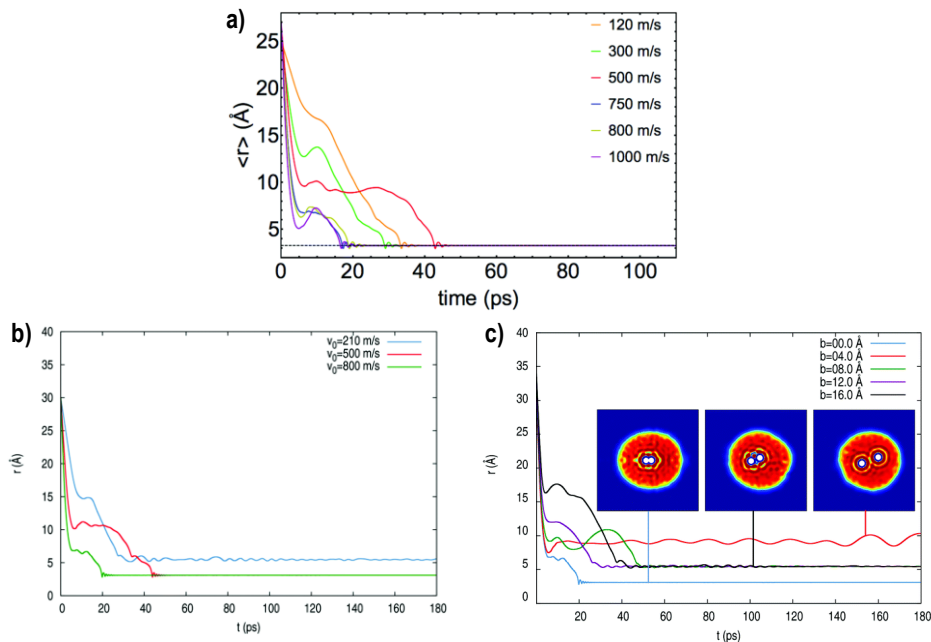
Figure 16. a) Average value of the distance between the neon wave packets vs time in the TDDFT/QM approach [78]. Distance of the neon atoms vs time with b) b=0 Å and c) $\langle v_0 \rangle = 800 \ m \cdot s^{-1}$, both in the TDDFT/CM approach. [79]

We can see a comparison of the results obtained using the TDDFT/CM and TDDFT/QM methods in Figure 16. Figure 16a corresponds to the TDDFT/QM approach, and shows that a dimer of bond distance 3.29 Å is obtained as a product regardless of the initial velocity. Contrarily, in the case where the impurities are treated classically (Figure 16b) the product obtained in the case of $\langle v_0 \rangle = 210 \ m \cdot s^{-1}$ corresponds to an adduct of bond distance equal to 5.45 Å. This pseudodimer is originated due to the lack of energy of the atoms to push away the helium density that separates them. Thus, a clear difference is found between the two approaches. The quantum approach predicts a slightly lower energy transfer from the colliding impurity to the liquid, making it easier to push away the helium density located between both atoms.

Furthermore, cases with angular momentum different from zero at $\langle v_0 \rangle = 800 \ m \cdot s^{-1}$ can be seen in Figure 16c. The appearance of the pseudodimer of bond distance equal to 5.45 Å is found again for impact parameters of 8, 12 and 16 Å. Interestingly, for b=4 Å another product is found. In this case the neon atoms are both fully and independently solvated, separated from

each other by ~9.14 Å. We can conclude that the system behaves in a non-monotonic way, making it difficult to extract clear tendencies on the outcome of the reaction. The waves generated in the liquid helium at the moment of collision may collide back to the impurities, changing their trajectories in ways hard to predict.

The introduction of angular momentum effectively reduces the velocity of the atoms in the reaction coordinate, making it harder to remove the helium density that separates them. In fact, there was not a single case where the impact parameter was different from zero that resulted in the 3.29 Å dimer. Moreover, the appearance of quantum vortices was reported in cases where the angular momentum was high enough, likewise to the capture scenario.

These dynamic results are in line with the static calculations reported by J. Eloranta (Figure 11, see section 6.1.1), which suggested the existence of neon adducts and quantum foams. Due to the very low temperature of the helium nanodroplets together with its capacity of rapidly releasing the excess energy, metastable products separated by layers of helium density can be found.

Dynamic calculations allow to find both the reaction products and reaction times. Furthermore, the microscopic mechanism of the reaction and the processes leading to its outcome can be thoroughly studied, e.g. the generation of waves and vortices in the helium due to the energy transfer mechanism upon collision.

Using the hybrid approach involving TDDFT for helium and classical mechanics for impurities several processes have been studied. In fact, this approach is the most common to perform dynamic simulations involving superfluid helium.

F. Coppens *et al.* [80,81] studied the formation and dynamics of $RbHe_N$ exciplexes, which are complexes generated in excited states of the impurity. By considering excitations to different electronic states of the rubidium atoms, which reside in the surface of the droplets, two different desorption regimes where found. One occurred in 30 ps, while the other one was found to take around 700 ps. In combination with experimental results, the authors were able to identify which excitations corresponded to each of the regimes. Besides, further excitations to heliophilic states were found to fall back to the droplet.

A similar process is the ejection of heliophilic atoms when excited to heliophobic states. This was studied by D. Mateo *et al.* [82] and the results obtained agree qualitatively with the

experimental results. Besides, they were able to predict the shifts observed in the spectroscopic results by static calculations.

Apart from the experimental investigation on the dynamics of the In atom ejection upon excitation [36,37] (see section 5.5.1), the authors included a theoretical study where the TDDFT/CM method was used to obtain further insight on the microscopic mechanism. The simulations were able to reproduce the bubble expansion, oscillations, ejection of the atom and the energy of the photoelectrons produced after ionization with the probe laser.

Another work by Coppens *et al.* [83] aimed at the effects of quantum vortices in the capture of several Ag atoms. It was found that the vortices trapped the atoms once they were travelling at low velocities, altering significantly the trajectories of the atoms. In some cases, the atoms were brought together, in others they were drifted apart. An example of snapshots of one of their calculation can be seen in Figure 17.

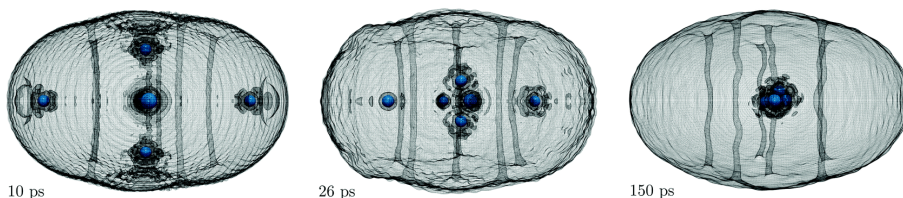10 ps   26 ps   150 ps

Figure 17. Snapshots of a nanodroplet with 6 quantum vortices and 6 Ag atoms being captured. [83]

Major differences were found when comparing the capture dynamics of heliophilic (Xe) and heliophobic (Cs) atoms. In the xenon case, a solvation layer was rapidly formed while in the other case this structure was not formed. When xenon atoms had enough initial speed to go through the droplet they carried with them some helium density. Again, this differed completely from the cesium case [84].

6.2.2.1. Ehrenfest Approximation

Overall, the TDDFT/CM method has proven to be a solid tool for studying processes involving doped helium nanodroplets. Treating the impurities classically does not exclude the possibility of working with different electronic states. In fact, it is common to account for several states using the Ehrenfest molecular dynamics approach.

Briefly, the Ehrenfest method describes the movement of the nuclei due to a potential resulting from the superposition of the different electronic states involved, which are averaged by coefficients that depend on time. Consequently, by analysing the changes of these coefficients

over time the transitions between the electronic states can be studied. A derivation of this method can be seen in section 3 of [85].

An example of use of this method is given by Y. Seki *et al.* [86] in a study of the ejection of a silver atom upon excitation from a low temperature cluster of 500 helium atoms. Ring polymer molecular dynamics were combined with the Ehrenfest approach, although the superfluid description of helium was not possible. By using this approach, they were not able to predict the final electronic state of the silver after the ejection, as their results did not match the experimental findings. However, the final Ag velocity distributions obtained roughly agreed with the experiment.

6.2.3. Instantaneous Helium Adaptation Approximation

A further approximation which can be done in dynamical calculations consists on assuming that the helium density instantly adapts to the impurity movement. In this approach the helium environment is treated as an energy correction in the interaction potential between the reactants.

A. W. Hauser *et al.* [87] followed this procedure to study the collision times of two impurities captured by a helium droplet, specifically, the Cu, Ag and Au atoms were considered. The helium environment was taken as a perturbation to the interaction potentials of the metals. This procedure is analogous to the one used in the study of the spatial quenching of the electron transfer reaction (Figure 12, see section 6.1.2). Besides to the inter-atomic interaction, the confinement potentials of the impurities were found by static calculations of singly doped droplets at different distances from the centre (Figure 18a).

Once the corrected interaction potentials and the confinement potentials were found, the Newton's equations of motion could be solved:

$$m_M \ddot{\boldsymbol{r}}_M = -\boldsymbol{\nabla}[V_{M-M'}(|\boldsymbol{r} - \boldsymbol{r}'|) + V_{M-He}(\boldsymbol{r})] \qquad (6.23)$$
$$m_M \ddot{\boldsymbol{r}}'_M = -\boldsymbol{\nabla}[V_{M-M'}(|\boldsymbol{r}' - \boldsymbol{r}|) + V_{M-He}(\boldsymbol{r}')] \qquad (6.24)$$

Where $\boldsymbol{r}$ and $\boldsymbol{r}'$ are the position vectors of the two impurities. The potential inducing the movement of each atom is given by the interaction with the other dopant ($V_{M-M'}$) and its interaction with the droplet (V_{M-He}). The simplification of the procedure allowed to perform thousands of calculations with random initial positions and with nanodroplets of up to 10000 helium atoms.

The approximations rely on the immediate adaptation of the helium density to the movement on the impurities, which only makes sense when the impurities travel below the Landau critical

velocity. Thus, in the simulation, the dopants are limited to go slower than 58 m·s^{-1}. The physical interpretation is simple, when this velocity is exceeded, friction will appear between the helium and the impurity, reducing its velocity until the Landau regime is reached again.

An example of the trajectories of the impurities through the droplet are shown in Figure 18b. Note how the trajectories are qualitatively equal to those showed in Figure 14b.

The distribution of the results obtained in the 10000 simulations performed for two copper atom impurities in a 5000 helium atoms droplet are shown in Figure 18c. Peaks with a periodicity of 130 ps are observed, which is the time it takes for a particle to traverse the nanodroplet at the Landau velocity. This relation was found in larger and smaller nanodroplets as well, leading to larger and smaller intervals respectively.
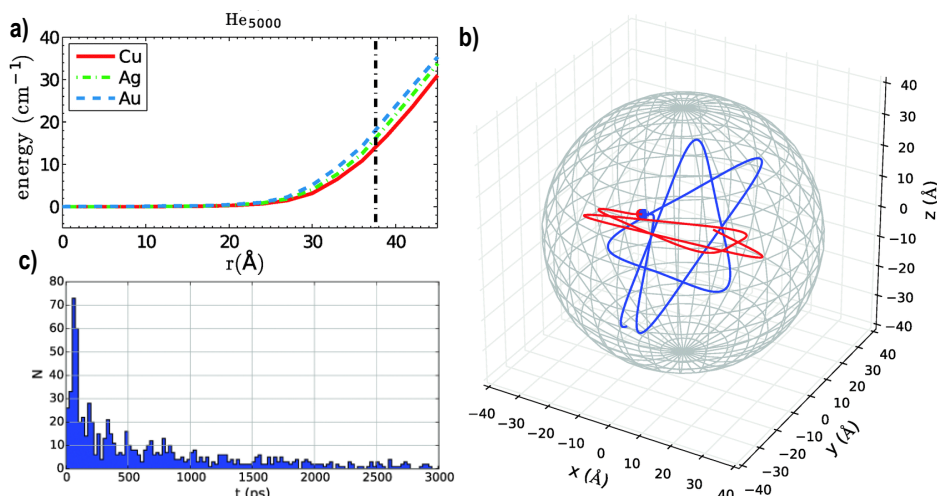
Figure 18. Result for a nanodroplet of 5000 helium atoms: a) Confinement potential. b) Trajectories of two Cu atoms. c) Results of 10000 simulations showing time collisions between two Cu atoms. A long tail beyond 3000 ps was cut for clarity. [87]

6.2.4. Basis Set Expansion

Now that the approximations that transform a quantum problem into a classical one have been explained, we can show a different way to simplify the quantum problem. There are some cases where further development of the motion equations that govern the system may transform them into others that can be propagated in a more efficient and accurate way.

If the process studied can be thought as one of the basic quantum mechanical problems (in essence, a harmonic oscillator or a rigid rotor) it may be possible to use the eigenfunctions of these systems as a basis to describe the problem of interest. To display how this idea may be applied we take as an example the work of M. Blancafort-Jorquera *et al.* on the rotational relaxation of a dimer inside a helium nanodroplet [88].

The aim of the study was to investigate the dynamics of the rotational relaxation process of a previously excited homonuclear diatomic molecule inside a helium droplet. The governing equations of the system, which are analogous to (6.15) and (6.16), are:

$$i\hbar \frac{\partial}{\partial t} \psi_{He} = \left[-\frac{\hbar^2}{2m_{He}} \nabla^2 + \iint \sin\theta \, d\theta d\phi V_{He-X_2}(\theta, \phi, \mathbf{R}_{He}) \left| \varphi_{X_2}(\theta, \phi) \right|^2 + \frac{\delta \mathcal{E}_c}{\delta \rho} \right] \psi_{He} \quad (6.25)$$

$$i\hbar \frac{\partial}{\partial t} \varphi_{X_2} = \left[-\frac{\hbar^2}{2I} \hat{L}^2 + \int d\mathbf{R}_{He} \, V_{He-X_2}(\theta, \phi, \mathbf{R}_{He}) \rho(\mathbf{R}_{He}) \right] \varphi_{X_2} \quad (6.26)$$

Where $I = \mu_{X_2} r_{eq,X_2}^2$ and $\hat{L}$ is the angular momentum operator. These equations refer to a helium droplet described by $\psi_{He}(\mathbf{R}_{He})$ and a dimer of reduced mass μ_{X_2} with a bond length constant and equal to r_{eq,X_2} described by $\varphi_{X_2}(\theta, \phi)$.

If we write the wave function of the dimer as $\varphi_{X_2}(\theta, \phi) = \sum c_{j,m_j} Y_{j,m_j}$, where Y_{j,m_j} are the spherical harmonics, we can modify (6.25) and (6.26) to obtain:

$$i\hbar \frac{\partial}{\partial t} \psi_{He} = \left[-\frac{\hbar^2}{2m_{He}} \nabla^2 + \sum_{i,m_i,j,m_j} c_{i,m_i}^* c_{j,m_j} V_{i,m_i,j,m_j}(\mathbf{R}_{He}) + \frac{\delta \mathcal{E}_c}{\delta \rho} \right] \psi_{He} \quad (6.27)$$

$$i\hbar \frac{\partial}{\partial t} c_{i,m_i} = E_{rot,i,m_i} c_{i,m_i} + \sum_{j,m_j} c_{j,m_j} V_{i,m_i,j,m_j} \quad (6.28)$$

Where $i = 1,2,\dots,n$, $m_i = -i,\dots,0,\dots,i$, and n determines how many basis functions we are using and:

$$V_{i,m_i,j,m_j}(\mathbf{R}_{He}) = \iint \sin\theta \, d\theta d\phi \, V_{He-X_2}(\theta, \phi, \mathbf{R}_{He}) Y_{i,m_i}^*(\theta, \phi) Y_{j,m_j}(\theta, \phi) \quad (6.29)$$

$$V_{i,m_i,j,m_j} = \iint \sin\theta \, d\theta d\phi \, d\mathbf{R}_{He} V_{He-X_2}(\theta, \phi, \mathbf{R}_{He}) \rho(\mathbf{R}_{He}) Y_{i,m_i}^*(\theta, \phi) Y_{j,m_j}(\theta, \phi) \quad (6.30)$$

The molecular wave function is a lineal combination of spherical harmonics, which are the solutions of the rigid rotor system (i.e., the free molecule), and its value will be determined at each moment of the evolution by the coefficients c_{i,m_i}, that depend on time. Physically, we can interpret this approach as the helium environment perturbating an otherwise freely rotating molecule.

Calculations were performed considering a sudden excitation from $j = 0$ and $m_j = 0$ to a higher rotational state and, then, the system was left to evolve to observe how it returned to the ground state. Hydrogen (H_2) and five more isotopes were considered (D_2, T_2, Qa_2, Qi_2 and Sx_2), where the first two are deuterium and tritium and the last three are hypothetical molecules with rotational constants of $1/4$, $1/5$ and $1/6$ the rotational constant of hydrogen. This made possible to study the effect of the rotational constant in the relaxation process.

As stated previously, the rotational relaxation process may require quite a lot of time to take place. Thus, optimizing the calculations is of the utmost importance. Previous calculations were used to understand which factors are truly important and to which extent.

For instance, the size of the nanodroplet has a major impact in the computational resources needed, and a study of its effect was performed. The structures of nanodroplets of different sizes are depicted in Figure 19a. It is readily seen how the second solvation layer changes very slightly from 100 to 125 helium atoms. As the rotational relaxation was predicted to be mostly affected by the interaction of the dopant with the closest solvation layers, adding more than a hundred helium atoms was not necessary, as their effect on the process would be minimal. A dynamical test was performed in Figure 19b to verify that the effect of the helium environment is small when more than 100 atoms are considered in the calculation.

Once the initial conditions for each calculation were found by static calculations, equations (6.27) and (6.28) were propagated over the real time and the evolution of the system could be found. The relaxation of the molecules to the $j = 0, m_j = 0$ state when excited to the $j = 2, m_j = 0$ level is illustrated in Figure 20a. It is noticed that, the smaller the rotational constant, the faster the molecule relaxes to the ground state.
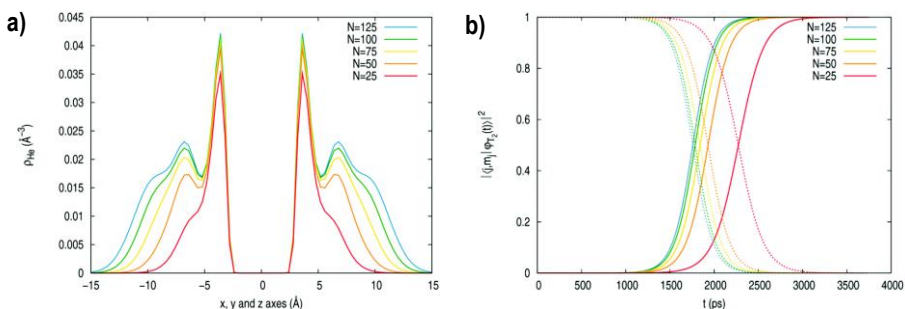

Figure 19. a) Helium radial density of the T_2 embedded in nanodroplets of N atoms. b) Populations of $T_2(j = 0, m_j = 0$, solid lines) and $T_2(j = 2, m_j = 0$, dashed lines) in droplets of N atoms over time. [88]
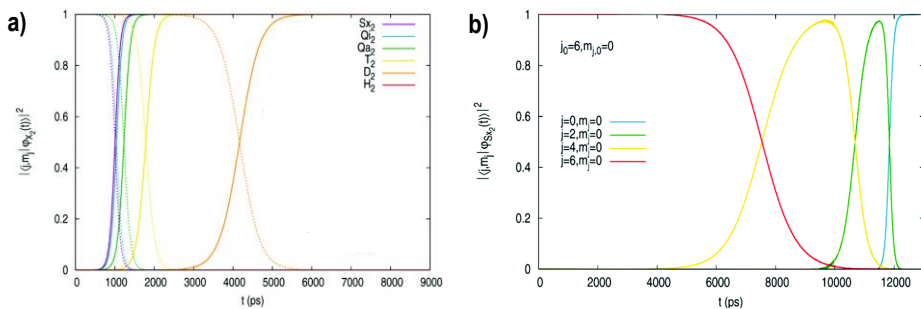
Figure 20. Populations of the rotational levels: a) molecules in the relaxation process from $j = 2, m_j = 0$ (dashed lines) to $j = 0, m_j = 0$ (solid lines). b) Sx_2 in the relaxation process from the $j = 6, m_j = 0$ to the ground state. Adapted from [88].

When the molecules were excited to higher energy states it was found that their metastability increased as the energy level increased (Figure 20b). The process of relaxation takes place almost in a cascade mechanism, where the de-excitation occurs *via* sequential steps. However, there is no metastability in the intermediate energy levels and each level begins to be populated before the previous de-excitation is completed.

Completely different results were found by A. Vilà *et al.* [89] where the same methodology was applied to the vibrational relaxation. In this case, the relaxation follows a true cascade mechanism, where the de-excitation takes place in steps and metastable states are found in all intermediate levels. In addition, it was found that the higher the excited state the faster the relaxation is, diverging again from the rotational process.

In both relaxations, the excess of energy of the molecule was transferred to the helium when it relaxed to lower energy levels (some helium density evaporated, releasing with it this energy excess). The differences between the rotational and vibrational relaxation processes were attributed to the very different nature of the motions involved. When exciting the molecule to higher vibrational states the amplitude of the oscillations increases, facilitating its interaction with the surrounding solvation layers and diminishing its lifetime. In contrast, the metastability of the rotational states increases the higher their energy is, and the authors concluded that the energy transfer from the molecule to the helium becomes harder as the angular velocity increases.

Employing the basis set of an analytically solvable quantum mechanical process can be of use in doped superfluid helium studies, since the perturbation suffered by the impurities is small. Moreover, this approach optimizes the use of computational resources to a point where studies

of processes of the order of several nanoseconds are viable while maintaining the quantum nature of the dopants.

6.2.5. Path Integral Centroid Molecular Dynamics

A radically different method from the previously explained is the path integral centroid molecular dynamics (PICMD). Only two examples of use in helium nanodroplets were found in the literature. T. Takayanagi and M. Shiga [90,91] studied the photodissociation of Cl_2 embedded in a droplet and the dynamics of KHe_N exciplexes.

In PICMD all the atoms of the system are considered semi-classically. Besides, the calculations in the literature simulate the system at 4 K. Hence, it does not account for the superfluidity of the liquid helium, which is expected to be one of the most important properties defining the behaviour of the system.

7. CONCLUSIONS

The chemical research involving superfluid helium nanodroplets has increased significantly during the last ten years. The development of synthetic methods to obtain complex nanostructures that are otherwise hard (or impossible) to obtain has been an important factor to understand this trend.

From the physical chemistry point of view, the application of fast pump-probe laser techniques has allowed to obtain a quite deep insight on the microscopic mechanisms and other dynamic properties of processes taking place in helium nanodroplets.

Thanks to the low interaction of the helium droplets with the dopants, theoretical structure calculations have provided a remarkable tool to elucidate the results of spectroscopic measurements.

Theoretical methods to investigate the dynamics of different physical and chemical phenomena occurring in Helium nanodroplets have been available only for the last five years. Due to the complexity of these systems, hybrid methods must be used, where the impurities (atoms or molecules) are described using quantum or classical mechanics and the helium nanodroplets are always considered using time dependent density functional theory.

The development of new experimental techniques in combination with the advances in theoretical simulations will allow to study doped helium nanodroplets extensively, yielding new knowledge on these systems about which there are still many questions to answer.

8. REFERENCES AND NOTES

[1]   Keesom, W. H. "Helium". *Elsevier*, **1942**.
[2]   Onnes, H. K. "Experiments on the Condensation of Helium by Expansion". *Commun Phys Lab Univ*, **1908**, *105*, 744.
[3]   Keesom, W. H.; Wolfke, M. "Two Different Liquid States of Helium". *Compt rend*, **1927**, *185*, 1465–1467.
[4]   Wolfke, M.; Keesom, W. H. "The Change of the Dielectric Constant of Liquid Helium with the Temperature. Provisional Measurements.". *Proc. Knin. Ned. Akad. van Wet.*, **1928**, *31*, 81–89.
[5]   Donnelly, R. J. "The Discovery of Superfluidity". *Phys. Today*, **1995**, *48*, 30–36.
[6]   Yang, S.; Ellis, A. M. "Helium Droplets: A Chemistry Perspective". *Chem. Soc. Rev.*, **2013**, *42*, 472–484.
[7]   Haynes, W. M. *CRC Handbook of Chemistry and Physics*; 97th ed.; **2017**.
[8]   Tisza, L. "Transport Phenomena in Helium II". *Nature*, **1938**, *141*, 913.
[9]   "Low Temperatures and Cold Molecules". **2008**.
[10]   Bogoliubov, N. N. "On the Theory of Superfluidity". *J. Phys. USSR*, **1942**, *11*, 23–32.
[11]   Becker, E. W. "On the History of Cluster Beams". *Z. Phys. Chem. D*, **1986**, *3*, 101–107.
[12]   Barranco, M.; Guardiola, R.; Hernández, S.; Mayol, R.; Navarro, J.; Pi, M. "Helium Nanodroplets: An Overview". *J. Low Temp. Phys.*, **2006**, *142*, 1–81.
[13]   Toennies, J. P.; Vilesov, A. F.; Whaley, K. B. "Superfluid Helium Droplets: An Ultracold Nanolaboratory". *Phys. Today*, **2001**, *54*, 31–37.
[14]   Scheidemann, A.; Toennies, J. P.; Northby, J. A. "Capture of Neon Atoms by ⁴He Clusters". *Phys. Rev. Lett.*, **1990**, *64*, 1899–1902.
[15]   Scheidemann, A.; Schilling, B.; Toennies, J. P.; Northby, J. A. "Capture of Foreign Atoms by Helium Clusters". *Phys. B Phys. Condens. Matter*, **1990**, *165–166*, 135–136.
[16]   Ancilotto, F.; Lerner, P. B.; Cole, M. W. "Physics of Solvation". *J. Low Temp. Phys.*, **1995**, *101*, 1123–1146.
[17]   Wiberley, S. E. "Mass Spectrometry". *J. Chem. Educ.*, **1964**, *41*, A75–A88.
[18]   Marty, M. T.; Beussman, D. J. "Simulating a Time-of-Flight Mass Spectrometer: A Labview Exercise". *J. Chem. Educ.*, **2013**, *90*, 239–243.
[19]   Krasnokutski, S. A.; Huisken, F. "Oxidative Reactions of Silicon Atoms and Clusters at Ultralow Temperature in Helium Droplets". *J. Phys. Chem. A*, **2010**, *114*, 13045–13049.
[20]   Lewerenz, M.; Schilling, B.; Toennies, J. P. "Successive Capture and Coagulation of Atoms and Molecules to Small Clusters in Large Liquid Helium Clusters". *J. Chem. Phys.*, **1995**, *102*, 8191.
[21]   "NIST Standard Reference Database 12.1"., **2019**.
[22]   Krasnokutski, S. A.; Huisken, F. "Low-Temperature Chemistry in Helium Droplets: Reactions of Aluminum Atoms with O_2 and H_2O". *J. Phys. Chem. A*, **2011**, *115*, 7120–7126.
[23]   Krasnokutski, S. A.; Kuhn, M.; Renzler, M.; Jäger, C.; Henning, T.; Scheier, P. "Ultra-Low-Temperature Reactions of Carbon Atoms With Hydrogen Molecules". *Astrophys. J.*, **2016**, *818*, L31.
[24]   Hartmann, M.; Miller, R. E.; Toennies, J. P.; Vilesov, A. "Rotationally Resolved Spectroscopy of SF_6 in Liquid Helium Clusters: A Molecular Probe of Cluster Temperature". *Phys. Rev. Lett.*, **1995**, *75*, 1566–1569.
[25]   Grebenev, S.; Toennies, J. P.; Vilesov, A. F. "Superfluidity within a Small Helium-4 Cluster: The Microscopic Andronikashvili Experiment". *Science*, **1998**, *279*, 2083–2086.
[26]   Franke, P. R.; Brice, J. T.; Moradi, C. P.; Schaefer, H. F.; Douberly, G. E. "Ethyl + O_2 in Helium Nanodroplets: Infrared Spectroscopy of the Ethylperoxy Radical". *J. Phys. Chem. A*, **2019**, *123*, 3558–3568.
[27]   Liang, T.; Douberly, G. E. "On the Al + HCN Reaction in Helium Nanodroplets". *Chem. Phys. Lett.*, **2012**, *551*, 54–59.
[28]   Brice, J. T.; Franke, P. R.; Douberly, G. E. "Sequential Capture of O(3P) and HCN by Helium Nanodroplets: Infrared Spectroscopy and Ab Initio Computations of the ³Σ O−HCN O-HCN Complex". *J. Phys. Chem. A*, **2017**, *121*, 9466–9473.
[29]   Nauta, K.; Miller, R. E. "Nonequilibrium Self-Assembly of Long Chains of Polar Molecules in Superfluid Helium". *Science*, **1999**, *283*, 1895–1897.
[30]   Habig, D.; Leicht, D.; Kaufmann, M.; Schwaab, G.; Havenith, M. "IR-Spectroscopic Study of the Allyl + NO Reaction in Helium Nanodroplets". *J. Chem. Phys.*, **2014**, *141*.
[31]   Krasnokutski, S. A.; Goulart, M.; Gordon, E. B.; Ritsch, A.; Jäger, C.; Rastogi, M.; Salvenmoser, W.; Henning, T.; Scheier, P. "Low-Temperature Condensation of Carbon". *Astrophys. J.*, **2017**, *847*, 1–7.
[32]   Thomas, B. J.; Harruff-Miller, B. A.; Bunker, C. E.; Lewis, W. K. "Infrared Spectroscopy of Mg-CO_2 and Al-CO_2 Complexes in Helium Nanodroplets". *J. Chem. Phys.*, **2015**, *142*, 174310.
[33]   Jia, L.; Le Brech, Y.; Mauviel, G.; Qi, F.; Bente-Von Frowein, M.; Ehlert, S.; Zimmermann, R.; Dufour, A. "Online Analysis

of Biomass Pyrolysis Tar by Photoionization Mass Spectrometry". *Energy and Fuels*, **2016**, *30*, 1555–1563.

[34] Loginov, E.; Rossi, D.; Drabbels, M. "Photoelectron Spectroscopy of Doped Helium Nanodroplets". *Phys. Rev. Lett.*, **2005**, *95*, 163401.

[35] Lindebner, F.; Kautsch, A.; Koch, M.; Ernst, W. E. "Laser Ionization and Spectroscopy of Cu in Superfluid Helium Nanodroplets". *Int. J. Mass Spectrom.*, **2014**, *365–366*, 255–259.

[36] Thaler, B.; Ranftl, S.; Heim, P.; Cesnik, S.; Treiber, L.; Meyer, R.; Hauser, A. W.; Ernst, W. E.; Koch, M. "Femtosecond Photoexcitation Dynamics inside a Quantum Solvent". *Nat. Commun.*, **2018**, *9*, 4006.

[37] Thaler, B.; Heim, P.; Treiber, L.; Koch, M. "Ultrafast Photoinduced Dynamics of Single Atoms Solvated inside Helium Nanodroplets". *J. Chem. Phys.*, **2020**, *152*, 014307.

[38] Thaler, B.; Meyer, M.; Heim, P.; Koch, M. "Long-Lived Nuclear Coherences inside Helium Nanodroplets". *Phys. Rev. Lett.*, **2020**, *124*, 115301.

[39] Wituschek, A. "Velocity Map Imaging". **2003**, *PhD Thesis*, 4–9.

[40] Bartels, C. "Angular Distributions of Photoelectrons from Cold , Size-Selected Sodium Cluster Anions". **2008**, *PhD Thesis*, 60–61.

[41] Sieg, A.; Von Vangerow, J.; Stienkemeier, F.; Dulieu, O.; Mudrich, M. "Desorption Dynamics of Rb$_2$ Molecules off the Surface of Helium Nanodroplets". *J. Phys. Chem. A*, **2016**, *120*, 7641–7649.

[42] Braun, A.; Drabbels, M. "Photodissociation of Alkyl Iodides in Helium Nanodroplets. I. Kinetic Energy Transfer". *J. Chem. Phys.*, **2007**, *127*, 114303.

[43] Braun, A.; Drabbels, M. "Photodissociation of Alkyl Iodides in Helium Nanodroplets. II. Solvation Dynamics". *J. Chem. Phys.*, **2007**, *127*, 114304.

[44] Braun, A.; Drabbels, M. "Photodissociation of Alkyl Iodides in Helium Nanodroplets. III. Recombination". *J. Chem. Phys.*, **2007**, *127*, 114305.

[45] Göde, S.; Irsig, R.; Tiggesbäumker, J.; Meiwes-Broer, K. H. "Time-Resolved Studies on the Collapse of Magnesium Atom Foam in Helium Nanodroplets". *New J. Phys.*, **2013**, *15*, 015026.

[46] Aguirre, N. F.; Mateo, D.; Mitrushchenkov, A. O.; Pi, M.; De Lara-Castells, M. P. "Helium Mediated Deposition: Modeling the He-TiO$_2$(110)-(1×1) Interaction Potential and Application to the Collision of a Helium Droplet from Density Functional Calculations". *J. Chem. Phys.*, **2012**, *136*, 1–14.

[47] Latimer, E.; Spence, D.; Feng, C.; Boatwright, A.; Ellis, A. M.; Yang, S. "Preparation of Ultrathin Nanowires Using Superfluid Helium Droplets". *Nano Lett.*, **2014**, *14*, 2902–2906.

[48] Gomez, L. F.; Loginov, E.; Vilesov, A. F. "Traces of Vortices in Superfluid Helium Droplets". *Phys. Rev. Lett.*, **2012**, *108*, 155302.

[49] Spence, D.; Latimer, E.; Feng, C.; Boatwright, A.; Ellis, A. M. "Vortex-Induced Aggregation in Superfluid Helium Droplets". **2014**, 6903–6906.

[50] Latimer, E.; Spence, D.; Feng, C.; Boatwright, A.; Ellis, A. M.; Yang, S. "Preparation of Ultrathin Nanowires Using Superfluid Helium Droplets". *Nano Lett.*, **2014**, *14*, 2902–2906.

[51] Emery, S. B.; Rider, K. B.; Little, B. K.; Schrand, A. M.; Lindsay, C. M. "Magnesium Cluster Film Synthesis by Helium Nanodroplets Magnesium Cluster Film Synthesis by Helium Nanodroplets". *J. Chem. Phys.*, **2013**, *139*, 054307.

[52] Wu, Q.; Ridge, C. J.; Zhao, S.; Zakharov, D.; Cen, J.; Tong, X.; Connors, E.; Su, D.; Stach, E. A.; Lindsay, C. M.; Orlov, A. "Development of a New Generation of Stable, Tunable, and Catalytically Active Nanoparticles Produced by the Helium Nanodroplet Deposition Method". *J. Phys. Chem. Lett.*, **2016**, *7*, 2910–2914.

[53] Hohenberg, P.; Kohn, W. "Inhomogeneous Electron Gas". *Phys. Rev.*, **1964**, *136*, B864–B871.

[54] Dalfovo, F.; Lastri, A.; Pricaupenko, L.; Stringari, S.; Treiner, J. "Structural and Dynamical Properties of Superfluid Helium: A Density-Functional Approach". *Phys. Rev. B*, **1995**, *52*, 1193–1209.

[55] Kosztin, I.; Faber, B.; Schulten, K. "Introduction to the Diffusion Monte Carlo Method". *Am. J. Phys.*, **1996**, *64*, 633–644.

[56] Lehtovaara, L.; Toivanen, J.; Eloranta, J. "Solution of Time-Independent Schrödinger Equation by the Imaginary Time Propagation Method". *J. Comput. Phys.*, **2007**, *221*, 148–157.

[57] Bader, P.; Blanes, S.; Casas, F. "Solving the Schrödinger Eigenvalue Problem by the Imaginary Time Propagation Technique Using Splitting Methods with Complex Coefficients". *J. Chem. Phys.*, **2013**, *139*.

[58] Eloranta, J. "Self-Assembly of Neon into a Quantum Gel with Crystalline Structure in Superfluid ^{4}He: Prediction from Density Functional Theory". *Phys. Rev. B*, **2008**, *77*, 134301.

[59] Eloranta, J. "Solvation of Atomic Fluorine in Bulk Superfluid ^{4}He". *Low Temp. Phys.*, **2011**, *37*, 491–493.

[60] Eloranta, J. "Theoretical Study of Quantum Gel Formation in Superfluid ^{4}He". *J. Low Temp. Phys.*, **2011**, *162*, 718–723.

[61] Paniagua, J. C.; Alemany, P. "Química Quàntica II. Segona edició.". Llibres de l'índex. **2015**.

[62] McQuarrie, D. A. "Quantum Chemistry". **2008**.

[63] Thaler, B.; Meyer, R.; Heim, P.; Ranftl, S.; Pototschnig, J. V; Hauser, A. W.; Koch, M.; Ernst, W. E. "Conservation of Hot Thermal Spin-Orbit Population of ^{2}P Atoms in a Cold Quantum Fluid Environment". *J. Phys. Chem. A*, **2019**, *123*, 3977–3984.

[64] Krasnokutski, S. A.; Huisken, F. "Ultra-Low-Temperature Reactions of C(^{3}P$_0$) Atoms with Benzene Molecules in Helium Droplets". *J. Chem. Phys.*, **2014**, *141*, 214306.

[65] Krasnokutski, S. A.; Huisken, F. "Ultra-Low-Temperature Reactions of Mg Atoms with O$_2$ Molecules in Helium Droplets

Serge". *J. Phys. Chem. A*, **2010**, *114*, 7292–7300.

[66]   Renzler, M.; Daxner, M.; Kranabetter, L.; Kaiser, A.; Hauser, A. W.; Ernst, W. E.; Lindinger, A.; Zillich, R.; Scheier, P.; Ellis, A. M. "Communication: Dopant-Induced Solvation of Alkalis in Liquid Helium Nanodroplets". *J. Chem. Phys.*, **2016**, *145*, 181101.

[67]   Hauser, A. W.; De Lara-Castells, M. P. "Spatial Quenching of a Molecular Charge-Transfer Process in a Quantum Fluid: The Cs: X-C$_{60}$ Reaction in Superfluid Helium Nanodroplets". *Phys. Chem. Chem. Phys.*, **2017**, *19*, 1342–1351.

[68]   De Lara-Castells, M. P.; Hauser, A. W.; Mitrushchenkov, A. O. "Ab Initio Confirmation of a Harpoon-Type Electron Transfer in a Helium Droplet". *J. Phys. Chem. Lett.*, **2017**, *8*, 4284–4288.

[69]   Ceperley, D. M. "Path Integrals in the Theory of Condensed Helium". *Rev. Mod. Phys.*, **1995**, *67*, 279–355.

[70]   Rodríguez-Cantano, R.; González-Lezana, T.; Villarreal, P. "Path Integral Monte Carlo Investigations on Doped Helium Clusters". *Int. Rev. Phys. Chem.*, **2016**, *35*, 37–68.

[71]   Pérez de Tudela, R.; Martini, P.; Goulart, M.; Scheier, P.; Pirani, F.; Hernández-Rojas, J.; Bretón, J.; Ortiz de Zárate, J.; Bartolomei, M.; González-Lezana, T.; Hernández, M.; Campos-Martínez, J.; Villarreal, P. "A Combined Experimental and Theoretical Investigation of Cs + Ions Solvated in He N Clusters". *J. Chem. Phys.*, **2019**, *150*, 154304.

[72]   Vilà, A.; González, M.; Mayol, R. "Quantum Dynamics of the Pick up Process of Atoms by Superfluid Helium Nanodroplets: The Ne + (^{4}He)$_{1000}$ System". *Phys. Chem. Chem. Phys.*, **2016**, *18*, 2006–2014.

[73]   Vilà, A.; González, M.; Mayol, R. "Photodissociation Dynamics of Homonuclear Diatomic Molecules in Helium Nanodroplets. the Case of Cl$_2$@(^{4}He)$_N$". *J. Chem. Theory Comput.*, **2015**, *11*, 899–906.

[74]   Vilà, A.; González, M.; Mayol, R. "Quantum Interferences in the Photodissociation of Cl$_2$(B) in Superfluid Helium Nanodroplets (^{4}He)$_N$". *Phys. Chem. Chem. Phys.*, **2015**, *17*, 32241–32250.

[75]   Vilà, A.; González, M.; Mayol, R. "Relaxation Dynamics of Helium Nanodroplets after Photodissociation of a Dopant Homonuclear Diatomic Molecule. The Case of Cl$_2$@(^{4}He)$_N$". *Phys. Chem. Chem. Phys.*, **2016**, *18*, 2409–2416.

[76]   Vilà, A.; González, M. "Mass Effects in the Photodissociation of Homonuclear Diatomic Molecules in Helium Nanodroplets: Inelastic Collision and Viscous Flow Energy Exchange Regimes". *Phys. Chem. Chem. Phys.*, **2016**, *18*, 27630–27638.

[77]   Blancafort-Jorquera, M.; Vilà, A.; González, M. "Quantum-Classical Dynamics of the Capture of Neon Atoms by Superfluid Helium Nanodroplets". *Phys. Chem. Chem. Phys.*, **2018**, *20*, 29737–29753.

[78]   Vilà, A.; González, M. "Reaction Dynamics inside Superfluid Helium Nanodroplets: The Formation of the Ne2 Molecule from Ne + Ne@(^{4}He)$_N$". *Phys. Chem. Chem. Phys.*, **2016**, *18*, 31869–31880.

[79]   Blancafort-Jorquera, M.; Vilà, A.; González, M. "Quantum-Classical Approach to the Reaction Dynamics in a Superfluid Helium Nanodroplet. The Ne$_2$ Dimer and Ne-Ne Adduct Formation Reaction Ne + Ne-Doped Nanodroplet". *Phys. Chem. Chem. Phys.*, **2019**, *21*, 24218–24231.

[80]   Coppens, F.; Von Vangerow, J.; Barranco, M.; Halberstadt, N.; Stienkemeier, F.; Pi, M.; Mudrich, M. "Desorption Dynamics of RbHe Exciplexes off He Nanodroplets Induced by Spin-Relaxation". *Phys. Chem. Chem. Phys.*, **2018**, *20*, 9309–9320.

[81]   Von Vangerow, J.; Coppens, F.; Leal, A.; Pi, M.; Barranco, M.; Halberstadt, N.; Stienkemeier, F.; Mudrich, M. "Imaging Excited-State Dynamics of Doped He Nanodroplets in Real-Time". *J. Phys. Chem. Lett.*, **2017**, *8*, 307–312.

[82]   Mateo, D.; Hernando, A.; Barranco, M.; Loginov, E.; Drabbels, M.; Pi, M. "Translational Dynamics of Photoexcited Atoms in ^{4}He Nanodroplets: The Case of Silver". *Phys. Chem. Chem. Phys.*, **2013**, *15*, 18388–18400.

[83]   Coppens, F.; Ancilotto, F.; Barranco, M.; Halberstadt, N.; Pi, M. "Dynamics of Impurity Clustering in Superfluid ^{4}He Nanodroplets". *Phys. Chem. Chem. Phys.*, **2019**, *21*, 17423–17432.

[84]   Coppens, F.; Leal, A.; Barranco, M.; Halberstadt, N.; Pi, M. "Head-on Collisions of Xe Atoms Against Superfluid 4He Nanodroplets". *J. Low Temp. Phys.*, **2017**, *187*, 439–445.

[85]   Paquet, E.; Viktor, H. L. "Computational Methods for Ab Initio Molecular Dynamics". *Adv. Chem.*, **2018**, *2018*, 1–14.

[86]   Seki, Y.; Takayanagi, T.; Shiga, M. "Photoexcited Ag Ejection from a Low-Temperature He Cluster: A Simulation Study by Nonadiabatic Ehrenfest Ring-Polymer Molecular Dynamics". *Phys. Chem. Chem. Phys.*, **2017**, *19*, 13798–13806.

[87]   Hauser, A. W.; Volk, A.; Thaler, P.; Ernst, W. E. "Atomic Collisions in Suprafluid Helium-Nanodroplets: Timescales for Metal-Cluster Formation Derived from He-Density Functional Theory". *Phys. Chem. Chem. Phys.*, **2015**, *17*, 10805–10812.

[88]   Blancafort-Jorquera, M.; Vilà, A.; González, M. "Rotational Energy Relaxation Quantum Dynamics of a Diatomic Molecule in a Superfluid Helium Nanodroplet and Study of the Hydrogen Isotopes Case". *Phys. Chem. Chem. Phys.*, **2019**, *21*, 21007–21021.

[89]   Vilà, A.; Paniagua, M.; González, M. "Vibrational Energy Relaxation Dynamics of Diatomic Molecules inside Superfluid Helium Nanodroplets. The Case of the I$_2$ Molecule". *Phys. Chem. Chem. Phys.*, **2017**, *20*, 118–130.

[90]   Takayanagi, T.; Shiga, M. "Photodissociation of Cl$_2$ in Helium Clusters: An Application of Hybrid Method of Quantum Wavepacket Dynamics and Path Integral Centroid Molecular Dynamics". *Chem. Phys. Lett.*, **2003**, *372*, 90–96.

[91]   Takayanagi, T.; Shiga, M. "Theoretical Study on Photoexcitation Dynamics of the K Atom Attached to Helium Clusters and the Solvation Structures of K*Hen Exciplexes". *Phys. Chem. Chem. Phys.*, **2004**, *6*, 3241–3247.

9. ACRONYMS

CM	Classical mechanics	QM	Quantum mechanics
DFT	Density functional theory	REMPI	Resonance-enhanced multiphoton ionization
HeND	Helium nanodroplet	TDDFT	Time dependent density functional theory
ITP	Imaginary time propagation	TDSE	Time dependent Schrödinger equation
MS	Mass spectrometry	TEM	Transmission electron microscopy
PES	Potential energy surface	TISE	Time independent Schrödinger equation
PICMD	Path integral centroid molecular dynamics	TOF	Time of flight
PIMC	Path Integral Monte Carlo	TOF-MS	Time of flight mass spectrometry